Differential effects of lysophospholipid headgroups, acyl chain length and saturation on vacuole acidification, Ca^{2+} transport, and fusion

Chi Zhang [1], Yilin Feng [1], Jorge D. Calderin [1], Adam Balutowski [1], Razeen Ahmed [1], Charlie Knapp [1], Ved Shah [1], Daniel Grudzien [1], Elizabeth Williamson [2], Jahnavi M. Karat [1] and Rutilio A. Fratti [1,2,*]

1. Deptartment of Biochemistry, University of Illinois Urbana-Champaign, Urbana, IL, 61801
2. Center for Biophysics and Quantitative Biology, University of Illinois Urbana-Champaign, Urbana, IL, 61801

* Correspondence: Rutilio A. Fratti (rfratti@illinois.edu)

Keywords: Acidification, Calcium, fusion, Lysophosphatidylcholine, Lysophosphatidic acid. SNARE, V-ATPase

ABSTRACT

SNARE-mediated membrane fusion is regulated by the lipid composition of the engaged bilayers. Lipids impact fusion through direct protein-lipid interactions or through modulating the physical properties of membranes to affect protein function. Lysophospholipids (LPLs) can affect membrane curvature, fluidity and energy of deformation. Their effects are due to their head group, and the length and saturation of their single acyl chains. Here we examined how the properties of LPLs affect yeast vacuole fusion and ion transport. We found that lysophosphatidylcholine (LPC) with acyl chains containing 14-18 carbons inhibited fusion with IC_{50} values of $\cong$ 40-120 μM. While acyl chain length moderately affected fusion, the head group played a major role. Unlike LPCs, Lysophosphatidic acid (LPA 18:1) failed to fully inhibit fusion, while lysophosphatidylethanolamine (LPE 18:1) had no effect. Separately we found that changes in acyl chain length and saturation differentially affected Ca^{2+} transport and vacuole acidification. Together these data show that the effects of LPLs on membrane fusion and ion transport were due to a combination of head group type and acyl chain length.

1 INTRODUCTION

Eukaryotes use SNARE-mediated membrane fusion to transport cargo between organelles as well as secretion at the plasma membrane (Bonifacino and Glick, 2004). Although the final stage of fusion is driven by SNAREs, the pathway is composed of multiple phases, each controlled by a distinct set of proteins and lipids. Membrane lipids can regulate protein function through two mechanisms. One mechanism is through specific interactions between lipids and proteins, as exemplified by the direct contacts of phosphoinositides (PIs) and lipid-binding protein domains (e.g., PH, PX, FYVE, etc.) (Lemmon, 2008; Balla, 2013; Overduin and Kervin, 2021). Another mode of regulation occurs through the effects of lipids on the physical properties of membranes including curvature, fluidity, thickness, and energy of deformation (Andersen and Koeppe, 2007; Harayama and Riezman, 2018; Levental and Lyman, 2023). These properties are affected by lipids such as cholesterol, sphingolipids, as well as glycerophospholipids with different acyl chain number, length and saturation, and head groups that vary in size and charge. Importantly, membrane curvature and fluidity can also be affected by lysophospholipids (LPL).

LPLs are generated through the action of various lipases and transferases. Lysophosphatidylcholine (LPC) can be generated by phospholipase-A1 (PLA1) or PLA2 on phosphatidylcholine (PC)

to release the fatty acid at the sn-1 or sn-2 position, leaving an LPC with a single acyl chain and an inverted cone shape due to the large headgroup and narrow tail (Grzelczyk and Gendaszewska-Darmach, 2013). LPC can also be made by LCAT (lecithin-cholesterol acyltransferase) and transfer of acyl chain to cholesterol. LPC can be converted to PC by LPCAT (LPC acyl transferase) (Zhang et al., 2021). Lysophosphatidic acid (LPA) is made by the action of intracellular and extracellular autotaxin (LysoPLD) on LPC (Salgado-Polo et al., 2018; Xie et al., 2024). LPA can also be made through a two component pathway of soluble PLA2-IIA and LysoPLD (Aoki et al., 2002b; Tsuboi et al., 2015; Tserendavga et al., 2021). Lysophosphatidylserine (LPS) is made by a PS-specific PLA1 to make sn-2 LPS which converts to sn-1 (Aoki et al., 2002a, 2002a). Lysophosphatidylethanolamine (LPE) is made by PLA1/2 (Makiyama et al., 2025) and LPI is made by DDHD1, which was previously identified as a PA preferring PLA1 (Yamashita et al., 2013).

LPLs can function as signaling molecules that act through binding all four classes of human GPCRs to trigger signal transduction cascades (Radeff-Huang et al., 2004; Li et al., 2016; Shanbhag et al., 2020). LPLs can also insert into membranes to induce positive curvature, thinning, and affect fluidity by disordering lipid packing (Razinkov et al., 1998; Fuller and Rand, 2001; Mishima et al., 2004). The degree of curvature is dependent on the length and saturation the acyl chain and headgroup. The smallest head group is a single phosphate on LPA. Larger headgroups range from ethanolamine (LPE), serine (LPS), choline (LPC) to inositol (LPI). The acyl chains of LPLs can range from 10-24 carbons that are saturated or contain one or more double bonds (Shanbhag et al., 2020).

LPLs are mostly resistant to bilayer translocation, i.e. Flip-Flopping, which prevents equilibration between leaflets. LPLs with 12 carbon chains or shorter can flip-flop across membrane leaflets (Seeman, 1972; Lieber et al., 1984), whereas longer LPLs do not readily flip lead to a pronounced increase in positive curvature. In erythrocytes, LPC can be generated on either side of the plasma membrane causing distinct morphological features (Mohandas et al., 1978). LPC generation on the outer leaflet produces protrusions (echinocytes), whereas production on the inner leaflet is stomatocytogenic causing the formation of pits or invaginations on the cell surface. In both cases, the deformation is caused by positive curvature induced by local LPC production (Mohandas et al., 1978). The degree of positive curvature can influence membrane protein function as shown by the >100 fold difference in the dimerization of gramicidin channels when comparing LPC and LPI (Lundbaek and Andersen, 1994). Induced positive curvature can also promote membrane

91 budding. Others have shown that ≥300 μM LPCs can produce bulges on 80 nm liposomes that
92 bud off as 20-30 nm vesicles after long incubations (Arouri and Mouritsen, 2013; Hua et al., 2023).
93 In yeast, LPI is enriched in COPII vesicles and promotes budding by increasing curvature and
94 reducing membrane rigidity (Melero et al., 2018).
95
96 In addition to membrane deformation, LPLs can affect ion channels that play critical roles in ho-
97 meostasis. For example, in erythrocytes LPA and LPCs regulate Ca^{2+}/Mg^{2+} ATPase function in a
98 manner dependent on acyl chain length and saturation, as well as headgroup type (Tokumura et
99 al., 1985). In HEK-293 cells the transient receptor potential (TRP) Ca^{2+} channel TRPC5 is acti-
100 vated by LPC and LPI with acyl chains with ≥14 carbons, whereas LPL 12:0 has no effect (Flem-
101 ming et al., 2006). Importantly, LPLs can affect Ca^{2+} transport in a protein-free manner through
102 the formation of transient Ca^{2+} pores as seen in lymphoma cells (Wilson-Ashworth et al., 2004).
103 LPLs can also trigger the opening of verapamil-sensitive L-type Ca^{2+} channels in monocytes (Lee
104 et al., 2006). Other LPL effects include regulating HL60 differentiation to macrophages, guanyl-
105 ate/adenylate cyclase activity, and insulin receptor auto-phosphorylation (Shier et al., 1976;
106 Asaoka et al., 1993; McCallum and Epand, 1995).
107
108 Altering membrane structure not only affects ion transport but can directly impact vesicle content
109 mixing as seen with the fusion of liposomes with cells (Wu et al., 1996), microsome fusion (Cher-
110 nomordik et al., 1993), or viral fusion (Chernomordik et al., 1997; Melikyan et al., 2000). Largely,
111 this occurs through affecting the formation and stability of hemifusion diaphragms and the transi-
112 tion to full bilayer fusion (Melikyan et al., 1997). LPCs can also affect fusion at the priming stage
113 when NSF activates SNAREs (Shin et al., 2012). The effect of LPLs on fusion can be compounded
114 by palmitoyl or stearoyl LPC inhibition of PLC-dependent diacylglycerol (DAG) generation, which
115 induces negative curvature needed for promoting the hemifusion to fusion transition (Okajima et
116 al., 1998; Goñi and Alonso, 1999; Villar et al., 2000).
117
118 Yeast vacuole homotypic fusion serves as a model in vitro system to examine the role of specific
119 proteins and lipids throughout the fusion cycle. Previous studies have mostly focused on glycer-
120 ophospholipids, sphingolipids (SL), and ergosterol on the different stages of fusion (Kato and
121 Wickner, 2001; Starr and Fratti, 2019; Zhang et al., 2024a). SNARE activation is regulated by the
122 conversion of phosphatidic acid to DAG, as well as the presence of ergosterol and $PI(4,5)P_2$
123 (Mayer et al., 2000; Kato and Wickner, 2001; Miner et al., 2016; Starr et al., 2019). Vacuole teth-
124 ering is regulated by the Rab Ypt7 and HOPS complex, which are both controlled by

125 phosphoinositides (PI) and SL (Stroupe et al., 2006; Cabrera et al., 2014; Lawrence et al., 2014;
126 Zhang et al., 2024a). Tethering leads to docking and SNARE pairing at distinct membrane micro-
127 domains that form interdependently with PI3P, PI(4,5)P_2, DAG, ergosterol and SL (Fratti et al.,
128 2004; Zhang et al., 2024a). The formation of SNARE complexes triggers the release of Ca^{2+} from
129 the vacuole lumen that is controlled in part by PI(3,5)P_2 (Merz and Wickner, 2004; Miner et al.,
130 2020). Prior to content mixing, vacuole outer leaflets undergo hemifusion which is affected by
131 DAG, PI(3,5)P_2, and LPC 12:0 (Reese and Mayer, 2005; Miner et al., 2019; Mondal et al., 2024).
132 Between hemifusion and fusion others have shown that the integral membrane Vo complex of the
133 V-ATPase can form dimers in trans between membranes in a LPC 12:0 sensitive manner (Peters
134 et al., 2001).
135
136
137 **2 Experimental procedures**
138 **2.1 Materials**
139 Reagents were solubilized in PIPES-Sorbitol (PS) buffer (20 mM PIPES-KOH, pH 6.8, 200 mM
140 sorbitol) with 125 mM KCl unless otherwise specified. Anti-Sec17 IgG (Mayer et al., 1996) and
141 Pbi2 (Slusarewicz et al., 1997) were prepared as previously described. ATP was purchased from
142 RPI (Mount Prospect, IL). Creatine phosphate was from Abcam (Waltham, MA). Acridine orange,
143 Coenzyme A (CoA), Creatine kinase, Triton X-100 (TX-100) and FCCP (Carbonyl cyanide-4-(tri-
144 fluoromethoxy) phenylhydrazone) were purchased from Sigma (St. Louis, MO) and dissolved in
145 PS buffer or DMSO. Cal-520 dextran conjugate MW, 10,000 (Cal-520) was from AAT Bioquest
146 (Sunnyvale, CA) and dissolved in DMSO. 1-myristoyl-2-hydroxy-sn-glycerol-3-phosphocholine
147 (LPC 14:0), 1-palmitoyl-2-hydroxy-sn-glycero-3-phosphocholine (LPC 16:0), 1-stearoyl-2-hy-
148 droxy-sn-glycero-3-phosphocholine (LPC 18:0), 1-oleoyl-2-hydroxy-sn-glycero-3-phosphocholine
149 (LPC 18:1), 1-oleoyl-2-hydroxy-sn-glycero-3-phosphatidic acid (sodium salt) (LPA 18:1), A23187,
150 and CCCP (carbonyl cyanide m-chlorophenyl hydrazone) were purchased from Cayman Chemi-
151 cal (Ann Arbor, MI) and dissolved in PS buffer or ethanol. 1-oleoyl-2-hydroxy-sn-glycero-3-phos-
152 phatidylethanolamine (LPE 18:1) was from Avanti Polar Lipids (Birmingham, AL) and dissolved in
153 ethanol.
154
155 **2.2 Vacuole isolation and in vitro content mixing**
156 Yeast vacuoles were isolated from BJ3505 (*pep4Δ PHO8)* and DKY6281 (*PEP4 pho8Δ*) as de-
157 scribed with modifications (Jones et al., 1982; Klionsky and Emr, 1989; Haas et al., 1994). Content
158 mixing reactions (30 µL) contained 3 µg each of vacuoles from BJ3505 and DKY6281

159 backgrounds in fusion reaction buffer composed of PS buffer, 125 mM KCl, 5 mM $MgCl_2$, ATP
160 regenerating system (ARS: 1 mM ATP, 0.1 mg/mL creatine kinase, 29 mM creatine phosphate),
161 10 μM CoA, and 280 nM recombinant Pbi2 (IB_2, Protease B inhibitor) (Slusarewicz et al., 1997).
162 The fusion of vacuoles mixes pro-Pho8 (inactive alkaline phosphatase) with the protease Pep4 to
163 make mature Pho8. Reactions were incubated at 27°C for 90 min and Pho8 activity was assayed
164 in 250 mM Tris-Cl, pH 8.5, 0.4% Triton X-100, 10 mM $MgCl_2$, 1 mM *p*-nitrophenyl phosphate.
165 Fusion was monitored as the absorbance at 400 nm from *p*-nitrophenolate production through
166 phosphatase activity.
167
168 **2.3 Fluorescence microscopy.**
169 Vacuole docking and vertex microdomain formation was performed as described (Sasser et al.,
170 2012b). Isolated vacuoles harboring Vps33-GFP were treated with 100 μM LPC 14:0, 50 μM LPC
171 16:0, 18:0 and 18:1, 150 μM LPA or PS buffer alone under docking conditions (PS buffer, 100
172 mM KCl, 0.5 mM $MgCl_2$, 0.33 mM ATP, 13 mM creatine phosphate, 33 μg/ml creatine kinase, 10
173 μM coenzyme A and 280 nM Pbi2) for 30 min at 27°C. After incubation, reactions were placed on
174 ice and membranes were labeled with 4 μM FM4-64 (Wang et al., 2002). Reactions were next
175 mixed with 20 μL 0.6% low melt agarose in PS buffer and mounted on microscope slides with
176 cover slips. Images were taken with a Zeiss Axio Observer Z1 inverted microscope with an X-Cite
177 120XL light source, Plane Apochromat 63X oil objective (NA 1.4) and an AxioCam 705 mono R2
178 CCD camera. Images were analyzed and heat maps were generated with ImageJ software (NIH).
179 Pseudo coloring and image merging was performed using Photoshop. s
180
181 **2.4 Calcium transport.**
182 Ca^{2+} transport across the vacuole membrane was detected with Cal-520 dextran conjugate (MW
183 10,000) as described previously (Sasser et al., 2012a; Miner and Fratti, 2019; Miner et al., 2020).
184 Ca^{2+} transport reactions (60 μl) contained 20 μg vacuoles isolated from BJ3505, reaction buffer,
185 10 μM CoA, 283 nM Pbi2, and 150 nM Cal-520. Reactions were transferred to wells of a black,
186 half-volume 96-well flat-bottom plate with nonbinding surface. Reactions were incubated at 27°C
187 for 5 min after which ARS was added to each well. For a negative control one well received addi-
188 tional PS buffer in lieu of ATP. Reactions were analyzed using a fluorescence plate reader (ex
189 485 nm and em 520 nm). SNARE-dependent Ca^{2+} efflux was blocked with antibody against the
190 SNARE co-chaperone Sec17. This served as a negative control for SNARE function (Merz and
191 Wickner, 2004). Fluorescence readings were taken every 30 s for 90 min and normalized to the
192 initial fluorescence value set to 1 for each reaction.

193

194 **2.5 Vacuole acidification**

195 Vacuole acidification was monitored by acridine orange (AO) fluorescence as described previ-
196 ously (Müller et al., 2003; Zhang et al., 2022a, 2022b). Individual reactions (60 µl) contained 20
197 µg BJ3505 vacuoles, reaction buffer, ARS, 10 µM CoA, 283 nM Pbi2, and 15 µM AO. Reactions
198 were set in a black half-volume 96-well flat-bottom plate with nonbinding surface. Test reagents
199 or PS buffer was added, and reactions were incubated at 27°C for 60 s after which ARS was
200 added to each well. One well received additional PS buffer in place of ATP to serve as a negative
201 control. AO fluorescence (ex 485 nm; em 520 nm) was measured in a fluorescence plate reader
202 and measurements were taken every 20 s. After AO fluorescence plateaued (400-600 s), each
203 well received 30 µM FCCP to collapse the proton gradient and restore AO fluorescence. Each
204 trace was normalized to their fluorescence intensities at the time of adding ATP and set to 1.

205

206 **2.5 Statistical analysis**

207 Results were expressed as the mean ± SE. Experimental replicates (n) are defined as the number
208 of separate experiments. Statistical analysis was performed by One-Way ANOVA for multiple
209 comparisons using Prism 10 (GraphPad, San Diego, CA). Tukey's post hoc analysis was used
210 for multiple comparisons and individual p-values. Statistical significance is represented as follows:
211 *p<0.05, ** p<0.01, *** p<0.001, **** p<0.0001.

212

213

214 **3 RESULTS**

215 **3.1 LPC and LPA inhibit vacuole fusion**

216 Previous studies showed that vacuole fusion can be inhibited by LPCs with C10-14 saturated
217 chains with IC_{50} values ranging from 30 µM for LPC 14:0 to ≅ 700 µM for LPC 10:0 (Reese and
218 Mayer, 2005). Earlier work by Chernomordik et al. found that LPC 14:0 inhibited cell-cell fusion
219 with and IC_{50} ≅ 10 µM and ≅ 1 µM for LPC 16:0 and LPC 18:0, respectively (Chernomordik et al.,
220 1997). Together these studies showed the importance of tail length in altering fusion efficiency.
221 Here we used LPCs containing C14-18 acyl chains. We also included the unsaturated LPC 18:1,
222 LPA 18:1 and LPE 18:1 to compare monounsaturation as well as head groups. LPS was excluded
223 due to the lack of solubility under fusion conditions. Vacuole fusion was determined by a content
224 mixing assay (Jones et al., 1982; Klionsky and Emr, 1989).

225

226 In these experiments we added concentration curves of LPLs at the start of the reaction and
227 incubated for 90 min at 27ºC. We found that vacuole fusion was inhibited by LPC 14:0 with an
228 IC_{50} of ≅ 120 μM **(Figure 1 A)**. When testing LPC 16:0 and LPC 18:0 we found that both inhibited
229 fusion with IC_{50} values of ≅ 45 μM **(Figure 1 B-C)**. This was higher than the Chernomordik et al.
230 study, however, a direct comparison is not possible due methodological differences and mem-
231 brane types. Their assay monitored the hemagglutinin-dependent plasma membrane fusion of
232 erythrocytes with HAb2 cells using R18 dequenching. This primarily measures outer leaflet fusion
233 (i.e., hemifusion) and not necessarily full content mixing. Our work tracked the SNARE-dependent
234 vacuole homotypic fusion using content mixing. Nevertheless, the level of fusion inhibition tracked
235 with the increase in acyl chain length.
236
237 We next asked if acyl chain saturation played a significant role in blocking fusion. To address this,
238 we used oleoyl LPC 18:1 (*cis*-Δ^9). Surprisingly, the unsaturation had no further effect as LPC 18:1
239 inhibited fusion with an IC_{50} ≅ 50 μM **(Figure 1 D)**. Finally, we examined the role of headgroup
240 type by comparing LPC 18:1 with LPA 18:1 and LPE 18:1. This showed that LPA affected vacuole
241 fusion but required a much higher concentration with an IC_{50} of ≅ 150 μM, which is an underesti-
242 mate since inhibition was only reduced by 60% **(Figure 1 E)**. Finally, we found that LPE 18:1 had
243 no effect on fusion **(Figure 1 F)**. This suggested that the head group of LPLs was more impactful
244 on fusion versus acyl chain length. The differences could be due to variances in induced positive
245 curvature. Both LPC and LPA are known to induce positive curvature, whereas LPE has no effect
246 on curvature (Fuller and Rand, 2001; Kooijman et al., 2005).
247
248 **3.2 LPC and LPA do not lyse vacuoles at levels that block fusion.**
249 Because LPLs can have detergent effects we tested if the inhibition of fusion vacuoles was due
250 to lysis. We used LPLs at their approximate IC_{50} values as well as concentrations that exceeded
251 these values. To probe for lysis, we pelleted membranes after the fusion reaction was complete
252 and collected the supernatant. Both membrane and supernatant fractions were probed by West-
253 ern blotting for the membrane anchored SNARE Nyv1. As a control for lysis, we used 1% TX-100.
254 In **Figure 1 G** we show that under control (PS) conditions Nyv1 was only in the membrane/pellet
255 (P) fraction apart from some background signal due to incomplete membrane re-isolation as well
256 as non-specific lysis during fusion (Starai et al., 2007). In contrast, Nyv1 was shifted to the super-
257 natant when vacuoles were treated with TX-100. No LPC variant lysed vacuoles at 50 and 125
258 μM. Nyv1 was only solubilized when LPC 16:0 and LPC 18:0 concentrations were at 250 μM
259 which was five-fold higher than their IC_{50} values. LPA had no effect on Nyv1 solubilization at any

concentration tested. Together, these data indicate that fusion inhibition was not due to lytic effects.

LPLs can act as detergents; however, this activity varies widely depending on the type of membrane (liposomes, purified organelles, whole cells, etc.), lipid composition, phase separation, and duration of exposure. For instance, LPC 18:0 can lyse microsomes but requires ≥400 μM, whereas erythrocytes are lysed in seconds by <20 μM LPCs (Weltzien, 1979; Tanaka et al., 1983; Chernomordik et al., 1993). Protein-free liposomes can be partially lysed by LPC with different acyl chains and dependent on osmolarity (Ralston et al., 1980; Senisterra et al., 1988). The ability of LPLs to permeabilize membranes can be counteracted by cholesterol, which in turn explains some of the differences between the susceptibility of artificial liposomes versus biological membranes (Arouri and Mouritsen, 2013). Another reason for such differences could be linked to the initial curvature of the experimental membrane so that smaller vesicles with high curvature are less disturbed by LPLs (Jespersen et al., 2012). For instance, fragile erythrocytes are 6-8 μm wide, while more resistant microsomes are 20-200 nm across and liposomes range from 50 nm to 100 μm. When considering true detergents, solubilization requires crossing bilayers to act on both leaflets, and full micellar solubilization can take hours (Kragh-Hansen et al., 1998; Hua et al., 2023).

3.3 LPLs do not affect vertex microdomain formation.

A study by Reese and Mayer showed that LPCs inhibited fusion after docking with moderate effects on trans-SNARE complex formation (Reese and Mayer, 2005). Thus, prior stages such as priming and docking were likely unaffected. That said, LPLs have been shown to alter microdomain size suggesting that vacuolar microdomains could be altered (Krasnobaev et al., 2022). During vacuole docking the lipids and proteins that drive fusion accumulate into vertex membrane microdomains and alterations in their assembly can inhibit downstream protein function (Wang et al., 2003; Fratti et al., 2004; Sasser et al., 2012b; Zhang et al., 2024b). Here we tested if LPLs at their IC_{50} concentrations altered vertex microdomain assembly. As a reporter we used vacuoles that contained Vps33-GFP, a subunit of the HOPS tethering complex (Wang et al., 2003). The vital dye FM4-64 was used to label the entirety of the docked membranes. Images were overlaid/merged to show where GFP and FM4-64 colocalized and heat maps were generated to show the intensities of GFP localization in relation to the other parts of the docked vacuoles. We found that Vps33-GFP enrichment at vertices was not affected by any of LPC or by LPA **(Figure 2)**. This

293 was consistent with the previous study showing that the effect of LPLs on fusion was downstream
294 of membrane docking.
295
296 **3.4 Ca^{2+} transport across the vacuole membrane is sensitive to LPLs**
297 Vacuoles are the main Ca^{2+} storage organelle in yeast, containing mM levels of the cation that is
298 mostly complexed to polyphosphate, leaving µM free Ca^{2+} available for transport (Dunn et al.,
299 1994). Vacuolar Ca^{2+} uptake utilizes the high affinity Ca-ATPase pump Pmc1 and the low affinity
300 Ca^{2+}/H^{+} (K^{+}/H^{+}) exchanger Vcx1 (Cunningham and Fink, 1994, 1996). Vacuoles also contain the
301 $PI(3,5)P_2$ sensitive TRP homolog Yvc1 that releases Ca^{2+} upon hyperosmotic stress-induced vac-
302 uole fission (Bonangelino et al., 2002; Denis and Cyert, 2002; Dong et al., 2010; Su et al., 2011).
303
304 During vacuole fusion SNAREs form complexes between membranes that leads to the release of
305 luminal Ca^{2+} (Merz and Wickner, 2004). This mechanism is independent of Yvc1, yet Ca^{2+} release
306 remains sensitive to levels of $PI(3,5)P_2$ (Miner et al., 2020). Since Ca^{2+} release during fusion was
307 likely mechanosensitive we next tested the effects of LPLs with a real-time fluorescence assay to
308 measure the kinetics of Ca^{2+} uptake and efflux (Sasser et al., 2012a; Miner and Fratti, 2019).
309 Extraluminal Ca^{2+} was detected with membrane impermeable Cal-520-dextran, which only fluo-
310 resces when bound to Ca^{2+}. Cal-520 fluorescence was high at the start of the reaction and rapidly
311 decreased after adding ATP to activate Ca^{2+} uptake. Upon trans-SNARE complex formation, Ca^{2+}
312 was released leading to an increase in fluorescence. As a control for efflux we included anti-
313 Sec17 IgG to prevent SNARE activation (Mayer et al., 1996). This allowed Ca^{2+} uptake without a
314 subsequent release. As a negative control for uptake, we included a reaction that lacked ATP
315 resulting in steady Cal-520 fluorescence.
316
317 To test the effects of LPLs on Ca^{2+} transport we added them at the start of the reactions, before
318 adding ATP to test their effects on uptake. Starting with LPC 14:0, we observed reduced Ca^{2+}
319 uptake as shown by the partial loss of fluorescence that stopped at 10 min and leveled off, thus
320 masking any effect on efflux at 30 min **(Figure 3 A-C)**. Based on the fusion data we imagined that
321 LPC 16:0 would have a stronger effect on Ca^{2+} uptake versus LPC 14:0. On the contrary, LPC
322 16:0 had no effect on Ca^{2+} uptake and resembled the untreated control **(Figure 3 D-F)**. While
323 uptake was not affected, LPC 16:0 completed blocked Ca^{2+} efflux at 125 µM and 250 µM and
324 partially blocked at 50 µM. When testing LPC-18:0 we found that it inhibited uptake to a greater
325 extent compared to LPC 14:0 **(Figure 3 G-I)**. The uptake of Ca^{2+} was inhibited by 250 µM LPC
326 18:0, while 125 µM kept uptake from reaching the anti-Sec17 plateau indicating that uptake was

327 partially blocked. The effect of 250 μM LPC 18:0 might be due to lysis whereas the effect of 125
328 μM LPC 18:0 likely masked any change in efflux. LPC 18:0 at 50 μM had no effect on uptake but
329 did cause a delay in efflux.
330
331 Next, we asked whether acyl chain saturation and head group affected Ca^{2+} transport. First, we
332 tested LPC 18:1 and found that it delayed and reduced uptake at 250 μM, but to a lesser extent
333 versus LPC 18:0 **(Figure 3 J-K)**. At lower concentrations LPC 18:1 did not significantly alter up-
334 take, however Ca^{2+} efflux at 30 min was inhibited **(Figure 3 J & L)**. This suggested that a mono-
335 unsaturation reduced the block of uptake while minimally changing the inhibition of efflux. Finally,
336 we asked if headgroup type would affect Ca^{2+} transport. To answer this, we used LPA 18:1 and
337 found that it had no effect on Ca^{2+} uptake or efflux when added at the beginning of the experiment
338 **(Figure 3 M-N)**. This indicated that the type of the head group played a critical role in altering
339 Ca^{2+} flux.
340
341 The effects of LPLs on Ca^{2+} uptake were not due to membrane permeabilization. In separate
342 experiments we tested the effects of TX-100 and the Ca^{2+} ionophore A23187. Adding TX-100 or
343 A23187 at the start of the reaction completely blocked Ca^{2+} uptake as measured by the lack of
344 fluorescence quenching of Cal-520 **(Supplemental Figure 1)**.
345
346 In previous studies we found that effects on Ca^{2+} uptake and efflux can be separated by varying
347 when an inhibitor is added (Miner et al., 2020). In Figure 2 we added LPLs at the start of the assay
348 and monitored both uptake at 10 min and efflux at 30 min. Some of the LPLs blocked uptake,
349 masking any effect on efflux later in the pathway. We next tested if LPLs could alter efflux when
350 added at 10 min after uptake was completed. Adding LPC 14:0 at 10 min led to a brief Ca^{2+}
351 release that was quickly reabsorbed **(Figure 4 A-B)**. We also observed delayed Ca^{2+} efflux for
352 ~10 min after which the reactions rapidly recovered to match the untreated control at 30 min
353 **(Figure 4 A-B)**. LPC 16:0 added at 10 min also caused a shortened efflux followed by a rapid
354 reuptake **(Figure 3C-D)**. However, unlike LPC 14:0, LPC 16:0 blocked Ca^{2+} efflux at the concen-
355 trations tested. Interestingly, LPC 18:0 had no striking effect on efflux even though the effect of
356 50 μM was statistically significant **(Figure 4 E-F)**. This showed that LPC 18:0 affected uptake but
357 not efflux. Together these data indicated that the most effective acyl chain length for altering Ca^{2+}
358 efflux was 16 carbons. Since IC_{50} values for inhibiting fusion were identical for LPC 16:0 and -
359 18:0, the difference in altering Ca^{2+} transport suggested that there was an additional effect trig-
360 gered by LPC 16:0 to alter the pathway.

361

362 Next, we tested if acyl chain saturation or head group size affected Ca^{2+} efflux. When added after
363 Ca^{2+} uptake was complete we found that 250 μM LPC 18:1 triggered a rapid rise in efflux **(Figure**
364 **4 G-H)**. This was likely due to partial lysis. After the rapid rise, the rate leveled off to match the
365 untreated control. Importantly, lower levels of LPC 18:1 potently inhibited Ca^{2+} efflux.
366

367 Lastly, we tested the late addition of LPA 18:1 on Ca^{2+} transport. When added at the start LPA
368 had no effect on uptake or efflux; however, when added after uptake was complete, we observed
369 a dose dependent inhibition of Ca^{2+} efflux **(Figure 4 I-J)**. This difference could be due to the
370 extraluminal Ca^{2+} concentration at the time of addition. For instance LPA forms type-1 lipid mi-
371 celles in the absence of divalent cations whereas the presence of divalent cations drives LPA to
372 form complexes with the cation in a bilayer (Kooijman et al., 2003).
373

374 Again, the inhibitory effects of LPLs on Ca^{2+} transport were not due to membrane permeabiliza-
375 tion. Ca^{2+} efflux was tested in the presence of TX-100 and A23187 added after Ca^{2+} uptake was
376 completed. Both TX-100 or A23187 caused a near-instant release of Ca^{2+} characterized by a
377 near vertical spike in Cal-520 fluorescence **(Supplemental Figure 1 A-B)**. To better observe the
378 signal spike, we added TX-100 and A23187 in the presence of anti-Sec17 to block natural SNARE
379 dependent Ca^{2+} efflux. This had no effect on Ca^{2+} release triggered by TX-100 and A23187 **(Sup-**
380 **plemental Figure 1 C-D)**.
381

382 **3.5 Vacuole acidification is inhibited by LPC**

383 Yeast vacuoles are acidic lysosomal compartments that aid in the degradation of macromolecules
384 into their constituent building blocks. This requires an acidic environment that activates digestive
385 enzymes at the site of activity and not during their trafficking through other organelles. Vacuole
386 acidification is primarily carried out by the vacuolar ATPase (V-ATPase) that is composed of two
387 complexes. The V_O complex is embedded in the membrane whereas the V_1 complex is cytoplas-
388 mic and can reversibly associate with the V_O to form the active holoenzyme (Vasanthakumar and
389 Rubinstein, 2020). The stability of V_1-V_O is promoted in part through the interactions of the V_O
390 subunit Vph1 and $PI(3,5)P_2$ (Li et al., 2014; Banerjee et al., 2019). Additionally, vacuole acidifica-
391 tion is attenuated by the lack of SL which increases fluidity and inhibits vacuole fusion (Zhang et
392 al., 2024a). The activity of V-ATPases is also sensitive to the fluidizing anesthetic dibucaine. Aside
393 from fluidity, we have found that acidification is sensitive to high Ca^{2+} (Zhang et al., 2022b). Based

394 on this and our data showing that LPLs can affect Ca^{2+} transport, we next asked if they could
395 affect vacuole acidification.
396
397 To measure vacuole acidification, we used AO which shifts fluorescence emission in acidic envi-
398 ronments (Moriyama et al., 1982). AO fluorescence shifts from 520 nm to 680 nm when trans-
399 ported in to the vacuole lumen (Pierzyńska-Mach et al., 2014; Thomé et al., 2016; Zhang et al.,
400 2022a). To test the effects of LPLs on acidification reactions were with run with buffer alone or
401 different concentrations of LPL for 30 sec after which ATP was added to start V-ATPase activity.
402 A separate reaction that lacked ATP served as a negative control. Reactions were run for 600 s
403 at which point 30 μM of the protonophore FCCP was added to each well to equilibrate H^+ concen-
404 trations across the membrane and restore AO fluorescence at 520 nm. This showed that the
405 decrease in fluorescence was indeed due to a proton gradient. In **Figure 5A** the black trace shows
406 the positive control with ATP and no LPC. The decrease in fluorescence plateaued at ~400 s after
407 the addition of ATP. In the absence of ATP, AO fluorescence was maintained throughout the
408 incubation (dotted trace). The addition of LPC 14:0 decreased the rate of acidification in a dose
409 dependent manner **(Figure 5 A-B)**. That said, each concentration of LPC 14:0 caught up with the
410 untreated control by 600 s. When we measured fluorescence at 400 s for multiple experiments,
411 we found that LPC 14:0 significantly attenuated H^+ transport (**Figure 5 B)**. This proportionally
412 matched its effect on Ca^{2+} uptake when added at T=0.
413
414 We next tested the effects of longer acyl chains on V-ATPase activity. Like LPC 14:0, the addition
415 of LPC 16:0 transiently slowed V-ATPase activity in a dose dependent manner that caught up
416 with the control by 600 s **(Figure 5 C-D)**. Interestingly, treating reactions with LPC 18:0 appeared
417 to stably inhibit V-ATPase activity as the treated samples never caught up with the control **(Figure**
418 **5 E-F)**. Together these data indicated that the V-ATPase was sensitive to acyl chain length. To
419 length alone was responsible for the effect, we used oleoyl LPC 18:1. We found that LPC 18:1
420 only slowed V-ATPase activity, and the treated samples caught up with the control as seen with
421 the with the shorter acyl chain containing LPCs **(Figure 5 G-H)**. This suggested that the narrowing
422 of stearoyl vs oleoyl hydrocarbons influenced the inhibition of V-ATPase activity. Lastly, we tested
423 LPA 18:1 and observed that vacuole acidification was unaffected **(Figure 5 I-J)**. This showed that
424 an oleoyl acyl chain alone was not sufficient in altering vacuole acidification. Instead, it appeared
425 that inhibiting V-ATPase function with LPLs was linked to the length of a saturated acyl chain and
426 the head group.
427

428 Finally, we examined the effect of adding LPLs after vacuole acidification had plateaued. We
429 found that LPC 14:0 had no significant effect on maintaining acidification levels **(Figure 6 A-B)**.
430 In contrast, LPC 16:0 **(Figure 6 C-D)**, LPC 18:0 **(Figure 6 E-F)** and LPC 18:1 **(Figure 6 G-H)** all
431 reversed V-ATPase activity as shown by the rise in AO fluorescence, albeit to different degrees.
432 This suggested that once acidified, maintaining the H^+ gradient was sensitive to acyl chains of 16
433 or more carbons in length and independent of hydrocarbon mono-unsaturation. Importantly, LPA
434 18:1 had no effect when added late matching its early addition **(Figure 6 I-J)**. This further indi-
435 cated that head group type was critical in the inhibition of vacuole acidification.
436
437 Similar to the effects of LPLs on Ca^{2+} transport, their effects on vacuole acidification were not
438 linked to lysis. In separate experiments we used TX-100 and different protonophore CCCP to test
439 acidification. As expected, the addition of either TX-100 or CCCP at the start of the reaction fully
440 blocked acidification **(Supplemental Figure 2)**. We also tested the effects of TX-100 and CCCP
441 after vacuole acidification was complete. For both reagents we observed a near vertical spike in
442 AO fluorescence, thus demonstrating that the effects of LPLs on acidification were not due to
443 lysis.
444
445 **4 DISCUSSION**
446 In this study we examined the role of LPLs on vacuole fusion, Ca^{2+} transport and V-ATPase ac-
447 tivity. Specifically, we tested the roles of acyl chain length and monounsaturation as well as head-
448 group type. In general, we found that the LPL traits tested had different effects on fusion and ion
449 transport. Apart from LPE, each of the LPLs inhibited vacuole fusion with varying efficacy. For
450 fusion the critical factor was headgroup type with LPA being less effective relative to the LPC
451 variants tested. The dependence on headgroup type suggested that differences in blocking fusion
452 could be due to the degree of positive curvature. While acyl chain length and saturation can further
453 affect curvature, it did not play a large role in blocking fusion. To illustrate the impact of head
454 group type, oleoyl LPC has a spontaneous positive curvature radius of +38 Å versus oleoyl LPA
455 with a radius of +20 Å in DOPE liposomes (Fuller and Rand, 2001; Kooijman et al., 2005). Pal-
456 mitoyl LPC has a curvature radius of +68 Å, illustrating how acyl chain saturation can further
457 influence membrane remodeling. On the other hand, LPE does not alter curvature in model mem-
458 branes. In addition to changes in curvature, it is possible that the negative charge of LPA influ-
459 ences how well fusion is blocked. For instance, the negative charge of LPA can interact with Ca^{2+}
460 to reduce its effect on curvature by inducing bilayer formation (Kooijman et al., 2003).
461

462 While the acyl chain length of 14-18 carbons made little difference in how well LPCs inhibited
463 fusion a study by Reese and Mayer looked at shorter acyl chain variants and found that inhibition
464 was relative to hydrocarbon length (Reese and Mayer, 2005). Specifically, they found that LPC-
465 14, -12, -10 and -8 inhibited vacuole fusion with IC_{50} values of 30 μM, 100 μM, 400 μM, and 3
466 mM, respectively (Reese and Mayer, 2005). Together with our data, we can conclude that acyl
467 chain length is important until efficacy plateaus at 14C. Their study went on to show that the block
468 in fusion was between SNARE pairing/hemifusion and content mixing. A critical step between
469 these phases is the release of luminal Ca^{2+} upon trans-SNARE complex formation (Merz and
470 Wickner, 2004). The effects of LPLs on Ca^{2+} transport have been shown with multiple transporters
471 in different cell types, however, these studies mostly focused on the plasma membrane and cy-
472 tosolic Ca^{2+}.
473
474 Among the types of Ca^{2+} transporters affected by LPLs are L-type voltage dependent channels.
475 In myocytes production of LPC stimulates L-type channels leading to Ca^{2+} overloading that was
476 inhibited by the L-type antagonist nimodipine (Golfman et al., 1999). The same is seen in Dro-
477 sophila S2 cells (Wang et al., 2015). This effect was only seen with LPC 18:0 and LPC 16:0,
478 whereas LPC 18:1, -18:2, -18:3 had no effect. Furthermore, LPE, LPA, LPI and LPS did not trigger
479 Ca^{2+} accumulation. Transport through L/P-type channels including the yeast Ca^{2+} P-type ATPase
480 are sensitive to channel blockers such as verapamil (Zhang et al., 2022b).
481
482 LPLs can also affect Ca^{2+} transport by mechanosensitive channels including members of the TRP
483 family. For example, TRPC5 is activated by LPC and LPI with acyl chains containing 14 or more
484 carbons (Flemming et al., 2006). That said the same study showed that LPLs had no effect on
485 TRPC2. LPC and LPI also induce Ca^{2+} influx via TRPv2 when the acyl chains were at least 16
486 carbons in length. This also led to increased cell migration in prostate cancer cells, suggesting
487 that actin dynamics were affected (Monet et al., 2009). In this case, headgroup type was also
488 considered and revealed that LPA and LPE had no effect. The effect of headgroup type is not
489 consistent as shown in lens cells where LPA triggers Ca^{2+} flux through a mechanosensitive chan-
490 nel, while LPC had no effect (Ohata et al., 1997). In these cases, LPL triggered transport through
491 mechanosensitive ion channels are not affected by inhibitors such as verapamil and nicardipine,
492 thapsigargin or blocking phospholipase-C with U73122.
493
494 So, how do LPLs affect yeast vacuole Ca^{2+} transport? Vacuoles move Ca^{2+} from the cytoplasm
495 to the lumen through the P-type ATPase Pmc1 and the Ca^{2+}/H^{+} antiporter Vcx1. Previously, we

496 showed that Ca^{2+} uptake is blocked by verapamil when added at T=0, which looks like the effects
497 of LPC 14:0 and LPC 18:0 and to a lesser extent LPC 18:1. On the other hand, LPC 16:0 and
498 LPA 18:1 have no effect on uptake whereas LPC 16:0 completely blocks Ca^{2+} efflux. This also
499 eliminates the possibility of causing lysis or transient pores to release Ca^{2+} as seen in lymphoma
500 cells (Wilson-Ashworth et al., 2004). When added late in the reaction we previously showed that
501 verapamil caused a rapid release of Ca^{2+}, suggesting that Pmc1 activity normally continues
502 throughout the reaction in part to balance the release of Ca^{2+}. Otherwise, only LPC 16:0 and LPA
503 18:1 were able to block Ca^{2+} efflux. LPC 18:1 blocked Ca^{2+} release at 50 and 125 μM whereas
504 250 μM triggered a rapid release. The later could be attributed to lysis whereas the former indi-
505 cates that efflux was truly inhibited.
506
507 Regarding acidification, we believe this is likely occurring through changes in curvature and/or
508 fluidity. V-ATPase activity has been linked to its interactions with cholesterol-rich microdomains
509 in tumor cells (Costa et al., 2018). Depletion of cholesterol with methyl-β-cyclodextrin, therfore
510 increasing fluidity reduced pumping activity as well as rates of cell migration. In our hands, in-
511 creasing fluidity with dibucaine or SL attenuates V-ATPase function (Zhang et al., 2024a).
512
513 Could LPLs interdependently affect Ca^{2+} and H^+ transport? We previously showed that vacuole
514 acidification was interdependent with Ca^{2+} gradients (Zhang et al., 2022b). The addition of Ca^{2+}
515 to AO assays inhibits V-ATPase function that is dependent on the Ca^{2+}/H^+ exchanger Vcx1 (Zhang
516 et al., 2022b). Conversely, Ca^{2+} transport required vacuole acidification. Both chloroquine and the
517 V-ATPase inhibitor Bafilomycin block Ca^{2+} uptake and maintaining the Ca^{2+} gradient. This raises
518 the question as to whether LPLs affect acidification and Ca^{2+} transport in a similar way. Proteomic
519 studies have shown that Vcx1 physically interacts with the V_O subunits Vma6 and Vph1, as well
520 as the V_1 subunits Vma1, Vma2, Vma4, Vma10 and Vma13 (Khan et al., 2022; Michaelis et al.,
521 2023). We found that LPC 14:0 blocks Ca^{2+} when added at T=0 min and not at T=10 min. This
522 correlates with blocked acidification when LPC 14:0 is added at T=0 min and not T= 500 s. Similar
523 effects are seen with LPC 18:0 and LPC 18:1, albeit to different degrees. These outcomes corre-
524 late with the role of Vcx1 Ca^{2+}/H^+ transport; however, it is not universal for all LPCs tested. When
525 looking at LPC 16:0, we saw that it did not affect Ca^{2+} uptake, yet it blocks acidification. A similar
526 relationship occurs when LPC 16:0 is added later in the reactions. Another inconsistency is seen
527 with LPA, which has no effect on Ca^{2+} or H^+ transport when added at T=0. When added late, LPA
528 can inhibit Ca^{2+} release and yet it has no effect on vacuole acidification. The lack of an effect on
529 acidification could be because Ca^{2+} did not accumulate outside the vacuole and instead was

retained in the lumen. These data suggest that the effects of LPLs on H^+/Ca^{2+} transport are not linked.

In conclusion, this study shows that vacuole fusion and ion transport can be differentially affected by LPCs depending on acyl chain length and to a lesser extent monounsaturation. We also report that headgroup type influences how LPLs affect fusion if they can also induce positive curvature.

Data Availability

Correspondence and requests for materials should be addressed to Rutilio Fratti (rfratti@illinois.edu)

Author Contribution

C.Z., R.A.F., designed the research; C.Z., Y.F. J.D.C, A.B., R.A, C.K., V.S., D.G. E.F. J.M.K. R.A.F., obtained the data; C.Z., R.A.F., formal analysis; C.Z., R.A.F., writing original draft; All authors reviewed and edited the manuscript; R.A.F., funding acquisition, supervision, project administration, resources.

Funding

This research was supported by grants from the National Science Foundation (MCB1818310 and MCB2216742 to RAF). JDC was partially supported by an NIGMS-NIH Chemistry-Biology Interface Training Grant (5T32-GM070421).

Conflict of interest

The authors declare that they have no conflict of interest.

Generative AI statement

The authors declare that generative AI was not used in the writing of this manuscript.

References

Andersen, O. S., and Koeppe, R. E. (2007). Bilayer thickness and membrane protein function: an energetic perspective. *Annu. Rev. Biophys. Biomol. Struct.* 36, 107–130. doi: 10.1146/annurev.biophys.36.040306.132643

563 Aoki, J., Nagai, Y., Hosono, H., Inoue, K., and Arai, H. (2002a). Structure and function of phos-
564 phatidylserine-specific phospholipase A1. *Biochim. Biophys. Acta* 1582, 26–32. doi:
565 10.1016/s1388-1981(02)00134-8

566 Aoki, J., Taira, A., Takanezawa, Y., Kishi, Y., Hama, K., Kishimoto, T., et al. (2002b). Serum
567 Lysophosphatidic Acid Is Produced through Diverse Phospholipase Pathways*. *J. Biol.*
568 *Chem.* 277, 48737–48744. doi: 10.1074/jbc.M206812200

569 Arouri, A., and Mouritsen, O. G. (2013). Membrane-perturbing effect of fatty acids and lysolipids.
570 *Prog. Lipid Res.* 52, 130–140. doi: 10.1016/j.plipres.2012.09.002

571 Asaoka, Y., Yoshida, K., Sasaki, Y., and Nishizuka, Y. (1993). Potential role of phospholipase
572 A2 in HL-60 cell differentiation to macrophages induced by protein kinase C activation.
573 *Proc. Natl. Acad. Sci. U. S. A.* 90, 4917–4921. doi: 10.1073/pnas.90.11.4917

574 Balla, T. (2013). Phosphoinositides: Tiny Lipids With Giant Impact on Cell Regulation. *Physiol.*
575 *Rev.* 93, 1019–1137. doi: 10.1152/physrev.00028.2012

576 Banerjee, S., Clapp, K., Tarsio, M., and Kane, P. M. (2019). Interaction of the late endo-lysoso-
577 mal lipid PI(3,5)P2 with the Vph1 isoform of yeast V-ATPase increases its activity and
578 cellular stress tolerance. *J. Biol. Chem.* 294, 9161–9171. doi:
579 10.1074/jbc.RA119.008552

580 Bonangelino, C. J., Nau, J. J., Duex, J. E., Brinkman, M., Wurmser, A. E., Gary, J. D., et al.
581 (2002). Osmotic stress-induced increase of phosphatidylinositol 3,5-bisphosphate re-
582 quires Vac14p, an activator of the lipid kinase Fab1p. *J. Cell Biol.* 156, 1015–1028. doi:
583 10.1083/jcb.200201002

584 Bonifacino, J. S., and Glick, B. S. (2004). The mechanisms of vesicle budding and fusion. *Cell*
585 116, 153–166. doi: 10.1016/s0092-8674(03)01079-1

586 Cabrera, M., Nordmann, M., Perz, A., Schmedt, D., Gerondopoulos, A., Barr, F., et al. (2014).
587 The Mon1-Ccz1 GEF activates the Rab7 GTPase Ypt7 via a longin-fold-Rab interface
588 and association with PI3P-positive membranes. *J. Cell Sci.* 127, 1043–1051. doi:
589 10.1242/jcs.140921

590 Chernomordik, L. V., Leikina, E., Frolov, V., Bronk, P., and Zimmerberg, J. (1997). An early
591 stage of membrane fusion mediated by the low pH conformation of influenza hemagglu-
592 tinin depends upon membrane lipids. *J. Cell Biol.* 136, 81–93. doi: 10.1083/jcb.136.1.81

593 Chernomordik, L. V., Vogel, S. S., Sokoloff, A., Onaran, H. O., Leikina, E. A., and Zimmerberg,
594 J. (1993). Lysolipids reversibly inhibit Ca(2+)-, GTP- and pH-dependent fusion of biologi-
595 cal membranes. *FEBS Lett.* 318, 71–76. doi: 10.1016/0014-5793(93)81330-3

596 Costa, G. A., de Souza, S. B., da Silva Teixeira, L. R., Okorokov, L. A., Arnholdt, A. C. V.,
597 Okorokova-Façanha, A. L., et al. (2018). Tumor cell cholesterol depletion and V-ATPase
598 inhibition as an inhibitory mechanism to prevent cell migration and invasiveness in mela-
599 noma. *Biochim. Biophys. Acta Gen. Subj.* 1862, 684–691. doi:
600 10.1016/j.bbagen.2017.12.006

601 Cunningham, K. W., and Fink, G. R. (1994). Calcineurin-dependent growth control in Saccharo-
602 myces cerevisiae mutants lacking PMC1, a homolog of plasma membrane Ca2+
603 ATPases. *J. Cell Biol.* 124, 351–363. doi: 10.1083/jcb.124.3.351

604 Cunningham, K. W., and Fink, G. R. (1996). Calcineurin inhibits VCX1-dependent H+/Ca2+ ex-
605 change and induces Ca2+ ATPases in Saccharomyces cerevisiae. *Mol. Cell. Biol.* 16,
606 2226–2237. doi: 10.1128/MCB.16.5.2226

607 Denis, V., and Cyert, M. S. (2002). Internal Ca(2+) release in yeast is triggered by hypertonic
608 shock and mediated by a TRP channel homologue. *J. Cell Biol.* 156, 29–34. doi:
609 10.1083/jcb.200111004

610 Dong, X., Shen, D., Wang, X., Dawson, T., Li, X., Zhang, Q., et al. (2010). PI(3,5)P(2) controls
611 membrane trafficking by direct activation of mucolipin Ca(2+) release channels in the en-
612 dolysosome. *Nat. Commun.* 1, 38. doi: 10.1038/ncomms1037

613 Dunn, T., Gable, K., and Beeler, T. (1994). Regulation of cellular Ca2+ by yeast vacuoles. *J.*
614 *Biol. Chem.* 269, 7273–7278.

615 Flemming, P. K., Dedman, A. M., Xu, S.-Z., Li, J., Zeng, F., Naylor, J., et al. (2006). Sensing of
616 lysophospholipids by TRPC5 calcium channel. *J. Biol. Chem.* 281, 4977–4982. doi:
617 10.1074/jbc.M510301200

618 Fratti, R. A., Jun, Y., Merz, A. J., Margolis, N., and Wickner, W. (2004). Interdependent assem-
619 bly of specific regulatory lipids and membrane fusion proteins into the vertex ring domain
620 of docked vacuoles. *J. Cell Biol.* 167, 1087–1098. doi: 10.1083/jcb.200409068

621 Fuller, N., and Rand, R. P. (2001). The Influence of Lysolipids on the Spontaneous Curvature
622 and Bending Elasticity of Phospholipid Membranes. *Biophys. J.* 81, 243–254. doi:
623 10.1016/S0006-3495(01)75695-0

624 Golfman, L. S., Haughey, N. J., Wong, J. T., Jiang, J. Y., Lee, D., Geiger, J. D., et al. (1999).
625 Lysophosphatidylcholine induces arachidonic acid release and calcium overload in car-
626 diac myoblastic H9c2 cells. *J. Lipid Res.* 40, 1818–1826.

627 Goñi, F. M., and Alonso, A. (1999). Structure and functional properties of diacylglycerols in
628 membranes. *Prog. Lipid Res.* 38, 1–48. doi: 10.1016/s0163-7827(98)00021-6

629 Grzelczyk, A., and Gendaszewska-Darmach, E. (2013). Novel bioactive glycerol-based lyso-
630 phospholipids: New data – New insight into their function. *Biochimie* 95, 667–679. doi:
631 10.1016/j.biochi.2012.10.009

632 Haas, A., Conradt, B., and Wickner, W. (1994). G-protein ligands inhibit in vitro reactions of vac-
633 uole inheritance. *J. Cell Biol.* 126, 87–97. doi: 10.1083/jcb.126.1.87

634 Harayama, T., and Riezman, H. (2018). Understanding the diversity of membrane lipid composi-
635 tion. *Nat. Rev. Mol. Cell Biol.* 19, 281–296. doi: 10.1038/nrm.2017.138

636 Hua, L., Kaiser, M., Carabadjac, I., Meister, A., Hause, G., and Heerklotz, H. (2023). Vesicle
637 budding caused by lysolipid-induced asymmetry stress. *Biophys. J.* 122, 4011–4022.
638 doi: 10.1016/j.bpj.2023.08.023

639 Jespersen, H., Andersen, J. H., Ditzel, H. J., and Mouritsen, O. G. (2012). Lipids, curvature
640 stress, and the action of lipid prodrugs: Free fatty acids and lysolipid enhancement of
641 drug transport across liposomal membranes. *Biochimie* 94, 2–10. doi: 10.1016/j.bio-
642 chi.2011.07.029

643 Jones, E. W., Zubenko, G. S., and Parker, R. R. (1982). PEP4 gene function is required for ex-
644 pression of several vacuolar hydrolases in Saccharomyces cerevisiae. *Genetics* 102,
645 665–677. doi: 10.1093/genetics/102.4.665

646 Kato, M., and Wickner, W. (2001). Ergosterol is required for the Sec18/ATP-dependent priming
647 step of homotypic vacuole fusion. *EMBO J.* 20, 4035–4040. doi: 10.1093/em-
648 boj/20.15.4035

649 Khan, M. M., Lee, S., Couoh-Cardel, S., Oot, R. A., Kim, H., Wilkens, S., et al. (2022). Oxidative
650 stress protein Oxr1 promotes V-ATPase holoenzyme disassembly in catalytic activity-
651 independent manner. *EMBO J.* 41, e109360. doi: 10.15252/embj.2021109360

652 Klionsky, D. J., and Emr, S. D. (1989). Membrane protein sorting: biosynthesis, transport and
653 processing of yeast vacuolar alkaline phosphatase. *EMBO J.* 8, 2241–2250.

654 Kooijman, E. E., Chupin, V., de Kruijff, B., and Burger, K. N. J. (2003). Modulation of membrane
655 curvature by phosphatidic acid and lysophosphatidic acid. *Traffic Cph. Den.* 4, 162–174.
656 doi: 10.1034/j.1600-0854.2003.00086.x

657 Kooijman, E. E., Chupin, V., Fuller, N. L., Kozlov, M. M., de Kruijff, B., Burger, K. N. J., et al.
658 (2005). Spontaneous curvature of phosphatidic acid and lysophosphatidic acid. *Bio-*
659 *chemistry* 44, 2097–2102. doi: 10.1021/bi0478502

660 Kragh-Hansen, U., le Maire, M., and Møller, J. V. (1998). The Mechanism of Detergent Solubili-
661 zation of Liposomes and Protein-Containing Membranes. *Biophys. J.* 75, 2932–2946.
662 doi: 10.1016/S0006-3495(98)77735-5

663 Krasnobaev, V. D., Galimzyanov, T. R., Akimov, S. A., and Batishchev, O. V. (2022). Lysolipids
664 regulate raft size distribution. *Front. Mol. Biosci.* 9. doi: 10.3389/fmolb.2022.1021321

665 Lawrence, G., Brown, C. C., Flood, B. A., Karunakaran, S., Cabrera, M., Nordmann, M., et al.
666 (2014). Dynamic association of the PI3P-interacting Mon1-Ccz1 GEF with vacuoles is
667 controlled through its phosphorylation by the type 1 casein kinase Yck3. *Mol. Biol. Cell*
668 25, 1608–1619. doi: 10.1091/mbc.E13-08-0460

669 Lee, Y.-K., Im, Y.-J., Kim, Y.-L., and Im, D.-S. (2006). Characterization of Ca2+ influx induced
670 by dimethylphytosphingosine and lysophosphatidylcholine in U937 monocytes. *Biochem.*
671 *Biophys. Res. Commun.* 348, 1116–1122. doi: 10.1016/j.bbrc.2006.07.164

672 Lemmon, M. A. (2008). Membrane recognition by phospholipid-binding domains. *Nat. Rev. Mol.*
673 *Cell Biol.* 9, 99–111. doi: 10.1038/nrm2328

674 Levental, I., and Lyman, E. (2023). Regulation of membrane protein structure and function by
675 their paralipidomes. *Nat. Rev. Mol. Cell Biol.* 24, 107–122. doi: 10.1038/s41580-022-
676 00524-4

677 Li, S. C., Diakov, T. T., Xu, T., Tarsio, M., Zhu, W., Couoh-Cardel, S., et al. (2014). The signal-
678 ing lipid PI(3,5)P_2 stabilizes V_1-V(o) sector interactions and activates the V-ATPase. *Mol.*
679 *Biol. Cell* 25, 1251–1262. doi: 10.1091/mbc.E13-10-0563

680 Li, Y.-F., Li, R.-S., Samuel, S. B., Cueto, R., Li, X.-Y., Wang, H., et al. (2016). Lysophospholip-
681 ids and their G protein-coupled receptors in atherosclerosis. *Front. Biosci. Landmark Ed.*
682 21, 70–88. doi: 10.2741/4377

683 Lieber, M. R., Lange, Y., Weinstein, R. S., and Steck, T. L. (1984). Interaction of chlorpromazine
684 with the human erythrocyte membrane. *J. Biol. Chem.* 259, 9225–9234. doi:
685 10.1016/S0021-9258(17)47289-9

686 Lundbaek, J. A., and Andersen, O. S. (1994). Lysophospholipids modulate channel function by
687 altering the mechanical properties of lipid bilayers. *J. Gen. Physiol.* 104, 645–673. doi:
688 10.1085/jgp.104.4.645

689 Makiyama, F., Kawase, S., Omi, A. W., Tanikawa, Y., Kotani, T., Shirayama, T., et al. (2025).
690 Differential effects of structurally different lysophosphatidylethanolamine species on pro-
691 liferation and differentiation in pre-osteoblast MC3T3-E1 cells. *Sci. Rep.* 15, 466. doi:
692 10.1038/s41598-024-84176-8

693 Mayer, A., Scheglmann, D., Dove, S., Glatz, A., Wickner, W., and Haas, A. (2000). Phosphati-
694 dylinositol 4,5-bisphosphate regulates two steps of homotypic vacuole fusion. *Mol. Biol.*
695 *Cell* 11, 807–817. doi: 10.1091/mbc.11.3.807

696 Mayer, A., Wickner, W., and Haas, A. (1996). Sec18p (NSF)-driven release of Sec17p (alpha-
697 SNAP) can precede docking and fusion of yeast vacuoles. *Cell* 85, 83–94. doi:
698 10.1016/s0092-8674(00)81084-3

699 McCallum, C. D., and Epand, R. M. (1995). Insulin receptor autophosphorylation and signaling
700 is altered by modulation of membrane physical properties. *Biochemistry* 34, 1815–1824.
701 doi: 10.1021/bi00006a001

702 Melero, A., Chiaruttini, N., Karashima, T., Riezman, I., Funato, K., Barlowe, C., et al. (2018).
703 Lysophospholipids Facilitate COPII Vesicle Formation. *Curr. Biol. CB* 28, 1950-1958.e6.
704 doi: 10.1016/j.cub.2018.04.076

705 Melikyan, G. B., Brener, S. A., Ok, D. C., and Cohen, F. S. (1997). Inner but not outer mem-
706 brane leaflets control the transition from glycosylphosphatidylinositol-anchored influenza
707 hemagglutinin-induced hemifusion to full fusion. *J. Cell Biol.* 136, 995–1005. doi:
708 10.1083/jcb.136.5.995

709 Melikyan, G. B., Markosyan, R. M., Hemmati, H., Delmedico, M. K., Lambert, D. M., and Cohen,
710 F. S. (2000). Evidence that the transition of HIV-1 gp41 into a six-helix bundle, not the
711 bundle configuration, induces membrane fusion. *J. Cell Biol.* 151, 413–423. doi:
712 10.1083/jcb.151.2.413

713 Merz, A. J., and Wickner, W. T. (2004). Trans-SNARE interactions elicit Ca2+ efflux from the
714 yeast vacuole lumen. *J. Cell Biol.* 164, 195–206. doi: 10.1083/jcb.200310105

Michaelis, A. C., Brunner, A.-D., Zwiebel, M., Meier, F., Strauss, M. T., Bludau, I., et al. (2023). The social and structural architecture of the yeast protein interactome. *Nature* 624, 192–200. doi: 10.1038/s41586-023-06739-5

Miner, G. E., and Fratti, R. (2019). Real-Time Fluorescence Detection of Calcium Efflux During Vacuolar Membrane Fusion. *Methods Mol. Biol. Clifton NJ* 1860, 323–331. doi: 10.1007/978-1-4939-8760-3_21

Miner, G. E., Starr, M. L., Hurst, L. R., Sparks, R. P., Padolina, M., and Fratti, R. A. (2016). The Central Polybasic Region of the Soluble SNARE (Soluble N-Ethylmaleimide-sensitive Factor Attachment Protein Receptor) Vam7 Affects Binding to Phosphatidylinositol 3-Phosphate by the PX (Phox Homology) Domain. *J. Biol. Chem.* 291, 17651–17663. doi: 10.1074/jbc.M116.725366

Miner, G. E., Sullivan, K. D., Guo, A., Jones, B. C., Hurst, L. R., Ellis, E. C., et al. (2019). Phosphatidylinositol 3,5-bisphosphate regulates the transition between trans-SNARE complex formation and vacuole membrane fusion. *Mol. Biol. Cell* 30, 201–208. doi: 10.1091/mbc.E18-08-0505

Miner, G. E., Sullivan, K. D., Zhang, C., Rivera-Kohr, D., Guo, A., Hurst, L. R., et al. (2020). Phosphatidylinositol 3,5-bisphosphate regulates Ca2+ transport during yeast vacuolar fusion through the Ca2+ ATPase Pmc1. *Traffic Cph. Den.* 21, 503–517. doi: 10.1111/tra.12736

Mishima, K., Nakajima, M., and Ogihara, T. (2004). Effects of lysophospholipids on membrane order of phosphatidylcholine. *Colloids Surf. B Biointerfaces* 33, 185–189. doi: 10.1016/j.colsurfb.2003.10.004

Mohandas, N., Greenquist, A. C., and Shohet, S. B. (1978). Bilayer balance and regulation of red cell shape changes. *J. Supramol. Struct.* 9, 453–458. doi: 10.1002/jss.400090315

Mondal, S., Pal, B., and Sankaranarayanan, R. (2024). Diacylglycerol metabolism and homeostasis in fungal physiology. *FEMS Yeast Res.* 24, foae036. doi: 10.1093/femsyr/foae036

Monet, M., Gkika, D., Lehen'kyi, V., Pourtier, A., Vanden Abeele, F., Bidaux, G., et al. (2009). Lysophospholipids stimulate prostate cancer cell migration via TRPV2 channel activation. *Biochim. Biophys. Acta* 1793, 528–539. doi: 10.1016/j.bbamcr.2009.01.003

Moriyama, Y., Takano, T., and Ohkuma, S. (1982). Acridine orange as a fluorescent probe for lysosomal proton pump. *J. Biochem. (Tokyo)* 92, 1333–1336. doi: 10.1093/oxfordjournals.jbchem.a134053

Müller, O., Neumann, H., Bayer, M. J., and Mayer, A. (2003). Role of the Vtc proteins in V-ATPase stability and membrane trafficking. *J. Cell Sci.* 116, 1107–1115. doi: 10.1242/jcs.00328

Ohata, H., Tanaka, K., Aizawa, H., Ao, Y., Iijima, T., and Momose, K. (1997). Lysophosphatidic acid sensitises Ca2+ influx through mechanosensitive ion channels in cultured lens epithelial cells. *Cell. Signal.* 9, 609–616. doi: 10.1016/s0898-6568(97)00066-1

753 Okajima, F., Sato, K., Tomura, H., Kuwabara, A., Nochi, H., Tamoto, K., et al. (1998). Stimula-
754 tory and inhibitory actions of lysophosphatidylcholine, depending on its fatty acid resi-
755 due, on the phospholipase C/Ca2+ system in HL-60 leukaemia cells. *Biochem. J.* 336,
756 491–500. doi: 10.1042/bj3360491

757 Overduin, M., and Kervin, T. A. (2021). The phosphoinositide code is read by a plethora of pro-
758 tein domains. *Expert Rev. Proteomics* 18, 483–502. doi:
759 10.1080/14789450.2021.1962302

760 Peters, C., Bayer, M. J., Bühler, S., Andersen, J. S., Mann, M., and Mayer, A. (2001). Trans-
761 complex formation by proteolipid channels in the terminal phase of membrane fusion.
762 *Nature* 409, 581–588. doi: 10.1038/35054500

763 Pierzyńska-Mach, A., Janowski, P. A., and Dobrucki, J. W. (2014). Evaluation of acridine or-
764 ange, LysoTracker Red, and quinacrine as fluorescent probes for long-term tracking of
765 acidic vesicles. *Cytom. Part J. Int. Soc. Anal. Cytol.* 85, 729–737. doi:
766 10.1002/cyto.a.22495

767 Radeff-Huang, J., Seasholtz, T. M., Matteo, R. G., and Brown, J. H. (2004). G protein mediated
768 signaling pathways in lysophospholipid induced cell proliferation and survival. *J. Cell. Bi-*
769 *ochem.* 92, 949–966. doi: 10.1002/jcb.20094

770 Ralston, E., Blumenthal, R., Weinstein, J. N., Sharrow, S. O., and Henkart, P. (1980). Lysophos-
771 phatidylcholine in liposomal membranes. Enhanced permeability but little effect on trans-
772 fer of a water-soluble fluorescent marker into human lymphocytes. *Biochim. Biophys.*
773 *Acta BBA - Biomembr.* 597, 543–551. doi: 10.1016/0005-2736(80)90226-6

774 Razinkov, V. I., Melikyan, G. B., Epand, R. M., Epand, R. F., and Cohen, F. S. (1998). Effects of
775 spontaneous bilayer curvature on influenza virus-mediated fusion pores. *J. Gen. Physiol.*
776 112, 409–422. doi: 10.1085/jgp.112.4.409

777 Reese, C., and Mayer, A. (2005). Transition from hemifusion to pore opening is rate limiting for
778 vacuole membrane fusion. *J. Cell Biol.* 171, 981–990. doi: 10.1083/jcb.200510018

779 Salgado-Polo, F., Fish, A., Matsoukas, M.-T., Heidebrecht, T., Keune, W.-J., and Perrakis, A.
780 (2018). Lysophosphatidic acid produced by autotaxin acts as an allosteric modulator of
781 its catalytic efficiency. *J. Biol. Chem.* 293, 14312–14327. doi:
782 10.1074/jbc.RA118.004450

783 Sasser, T. L., Padolina, M., and Fratti, R. A. (2012a). The yeast vacuolar ABC transporter Ybt1p
784 regulates membrane fusion through Ca2+ transport modulation. *Biochem. J.* 448, 365–
785 372. doi: 10.1042/BJ20120847

786 Sasser, T., Qiu, Q.-S., Karunakaran, S., Padolina, M., Reyes, A., Flood, B., et al. (2012b). Yeast
787 lipin 1 orthologue pah1p regulates vacuole homeostasis and membrane fusion. *J. Biol.*
788 *Chem.* 287, 2221–2236. doi: 10.1074/jbc.M111.317420

789 Seeman, P. (1972). The Membrane Actions of Anesthetics and Tranquilizers. *Pharmacol. Rev.*
790 24, 583–655.

791 Senisterra, G. A., Disalvo, E. A., and Gagliardino, J. J. (1988). Osmotic dependence of the lyso-
792 phosphatidylcholine lytic action on liposomes in the gel state. *Biochim. Biophys. Acta*
793 941, 264–270. doi: 10.1016/0005-2736(88)90187-3

794 Shanbhag, K., Mhetre, A., Khandelwal, N., and Kamat, S. S. (2020). The Lysophosphatidylser-
795 ines-An Emerging Class of Signalling Lysophospholipids. *J. Membr. Biol.* 253, 381–397.
796 doi: 10.1007/s00232-020-00133-2

797 Shier, W. T., Baldwin, J. H., Nilsen-Hamilton, M., Hamilton, R. T., and Thanassi, N. M. (1976).
798 Regulation of guanylate and adenylate cyclase activities by lysolecithin. *Proc. Natl.*
799 *Acad. Sci. U. S. A.* 73, 1586–1590. doi: 10.1073/pnas.73.5.1586

800 Shin, L., Wang, S., Lee, J.-S., Flack, A., Mao, G., and Jena, B. P. (2012). Lysophosphatidylcho-
801 line inhibits membrane-associated SNARE complex disassembly. *J. Cell. Mol. Med.* 16,
802 1701–1708. doi: 10.1111/j.1582-4934.2011.01433.x

803 Slusarewicz, P., Xu, Z., Seefeld, K., Haas, A., and Wickner, W. T. (1997). I2B is a small cyto-
804 solic protein that participates in vacuole fusion. *Proc. Natl. Acad. Sci. U. S. A.* 94, 5582–
805 5587. doi: 10.1073/pnas.94.11.5582

806 Starai, V. J., Jun, Y., and Wickner, W. (2007). Excess vacuolar SNAREs drive lysis and Rab by-
807 pass fusion. *Proc. Natl. Acad. Sci. U. S. A.* 104, 13551–13558. doi:
808 10.1073/pnas.0704741104

809 Starr, M. L., and Fratti, R. A. (2019). The Participation of Regulatory Lipids in Vacuole Homo-
810 typic Fusion. *Trends Biochem. Sci.* 44, 546–554. doi: 10.1016/j.tibs.2018.12.003

811 Starr, M. L., Sparks, R. P., Arango, A. S., Hurst, L. R., Zhao, Z., Lihan, M., et al. (2019). Phos-
812 phatidic acid induces conformational changes in Sec18 protomers that prevent SNARE
813 priming. *J. Biol. Chem.* 294, 3100–3116. doi: 10.1074/jbc.RA118.006552

814 Stroupe, C., Collins, K. M., Fratti, R. A., and Wickner, W. (2006). Purification of active HOPS
815 complex reveals its affinities for phosphoinositides and the SNARE Vam7p. *EMBO J.* 25,
816 1579–1589. doi: 10.1038/sj.emboj.7601051

817 Su, Z., Anishkin, A., Kung, C., and Saimi, Y. (2011). The core domain as the force sensor of the
818 yeast mechanosensitive TRP channel. *J. Gen. Physiol.* 138, 627–640. doi:
819 10.1085/jgp.201110693

820 Tanaka, Y., Mashino, K., Inoue, K., and Nojima, S. (1983). Mechanism of human erythrocyte
821 hemolysis induced by short-chain phosphatidylcholines and lysophosphatidylcholine. *J.*
822 *Biochem. (Tokyo)* 94, 833–840. doi: 10.1093/oxfordjournals.jbchem.a134425

823 Thomé, M. P., Filippi-Chiela, E. C., Villodre, E. S., Migliavaca, C. B., Onzi, G. R., Felipe, K. B.,
824 et al. (2016). Ratiometric analysis of Acridine Orange staining in the study of acidic orga-
825 nelles and autophagy. *J. Cell Sci.* 129, 4622–4632. doi: 10.1242/jcs.195057

826 Tokumura, A., Mostafa, M. H., Nelson, D. R., and Hanahan, D. J. (1985). Stimulation of (Ca2+ +
827 Mg2+)-ATPase activity in human erythrocyte membranes by synthetic lysophosphatidic
828 acids and lysophosphatidylcholines. Effects of chain length and degree of unsaturation

of the fatty acid groups. *Biochim. Biophys. Acta* 812, 568–574. doi: 10.1016/0005-2736(85)90332-3

Tserendavga, B., Ohshima, N., Fujita, C., Yuzawa, K., Ohshima, M., Yanaka, N., et al. (2021). Characterization of recombinant murine GDE4 and GDE7, enzymes producing lysophosphatidic acid and/or cyclic phosphatidic acid. *J. Biochem. (Tokyo)* 170, 713–727. doi: 10.1093/jb/mvab091

Tsuboi, K., Okamoto, Y., Rahman, I. A. S., Uyama, T., Inoue, T., Tokumura, A., et al. (2015). Glycerophosphodiesterase GDE4 as a novel lysophospholipase D: a possible involvement in bioactive *N*-acylethanolamine biosynthesis. *Biochim. Biophys. Acta BBA - Mol. Cell Biol. Lipids* 1851, 537–548. doi: 10.1016/j.bbalip.2015.01.002

Vasanthakumar, T., and Rubinstein, J. L. (2020). Structure and Roles of V-type ATPases. *Trends Biochem. Sci.* 45, 295–307. doi: 10.1016/j.tibs.2019.12.007

Villar, A. V., Alonso, A., and Goñi, F. M. (2000). Leaky vesicle fusion induced by phosphatidylinositol-specific phospholipase C: observation of mixing of vesicular inner monolayers. *Biochemistry* 39, 14012–14018. doi: 10.1021/bi992515c

Wang, L., Merz, A. J., Collins, K. M., and Wickner, W. (2003). Hierarchy of protein assembly at the vertex ring domain for yeast vacuole docking and fusion. *J. Cell Biol.* 160, 365–374. doi: 10.1083/jcb.200209095

Wang, L., Seeley, E. S., Wickner, W., and Merz, A. J. (2002). Vacuole fusion at a ring of vertex docking sites leaves membrane fragments within the organelle. *Cell* 108, 357–369. doi: 10.1016/s0092-8674(02)00632-3

Wang, P., Wang, Q., Yang, L., Qin, Q.-L., and Wu, Y.-J. (2015). Characterization of lysophosphatidylcholine-induced changes of intracellular calcium in Drosophila S2 cells. *Life Sci.* 131, 57–62. doi: 10.1016/j.lfs.2015.02.014

Weltzien, H. U. (1979). Cytolytic and membrane-perturbing properties of lysophosphatidylcholine. *Biochim. Biophys. Acta BBA - Rev. Biomembr.* 559, 259–287. doi: 10.1016/0304-4157(79)90004-2

Wilson-Ashworth, H. A., Judd, A. M., Law, R. M., Freestone, B. D., Taylor, S., Mizukawa, M. K., et al. (2004). Formation of transient non-protein calcium pores by lysophospholipids in S49 Lymphoma cells. *J. Membr. Biol.* 200, 25–33. doi: 10.1007/s00232-004-0691-x

Wu, H., Zheng, L., and Lentz, B. R. (1996). A slight asymmetry in the transbilayer distribution of lysophosphatidylcholine alters the surface properties and poly(ethylene glycol)-mediated fusion of dipalmitoylphosphatidylcholine large unilamellar vesicles. *Biochemistry* 35, 12602–12611. doi: 10.1021/bi960168q

Xie, Y., Ella, K. M., Gibbs, T. C., Yohannan, M. E., Knoepp, S. M., Balijepalli, P., et al. (2024). Characterization of Lysophospholipase D Activity in Mammalian Cell Membranes. *Cells* 13, 520. doi: 10.3390/cells13060520

Yamashita, A., Oka, S., Tanikawa, T., Hayashi, Y., Nemoto-Sasaki, Y., and Sugiura, T. (2013). The actions and metabolism of lysophosphatidylinositol, an endogenous agonist for

GPR55. *Prostaglandins Other Lipid Mediat.* 107, 103–116. doi: 10.1016/j.prostaglandins.2013.05.004

Zhang, C., Balutowski, A., Feng, Y., Calderin, J. D., and Fratti, R. A. (2022a). High throughput analysis of vacuolar acidification. *Anal. Biochem.* 658, 114927. doi: 10.1016/j.ab.2022.114927

Zhang, C., Calderin, J. D., Hurst, L. R., Gokbayrak, Z. D., Hrabak, M. R., Balutowski, A., et al. (2024a). Sphingolipids containing very long-chain fatty acids regulate Ypt7 function during the tethering stage of vacuole fusion. *J. Biol. Chem.* 0. doi: 10.1016/j.jbc.2024.107808

Zhang, C., Calderin, J. D., Hurst, L. R., Gokbayrak, Z. D., Hrabak, M. R., Balutowski, A., et al. (2024b). Sphingolipids containing very long-chain fatty acids regulate Ypt7 function during the tethering stage of vacuole fusion. *J. Biol. Chem.*, 107808. doi: 10.1016/j.jbc.2024.107808

Zhang, C., Feng, Y., Balutowski, A., Miner, G. E., Rivera-Kohr, D. A., Hrabak, M. R., et al. (2022b). The interdependent transport of yeast vacuole Ca2+ and H+ and the role of Phosphatidylinositol 3,5-bisphosphate. *J. Biol. Chem.*, 102672. doi: 10.1016/j.jbc.2022.102672

Zhang, Q., Yao, D., Rao, B., Jian, L., Chen, Y., Hu, K., et al. (2021). The structural basis for the phospholipid remodeling by lysophosphatidylcholine acyltransferase 3. *Nat. Commun.* 12, 6869. doi: 10.1038/s41467-021-27244-1

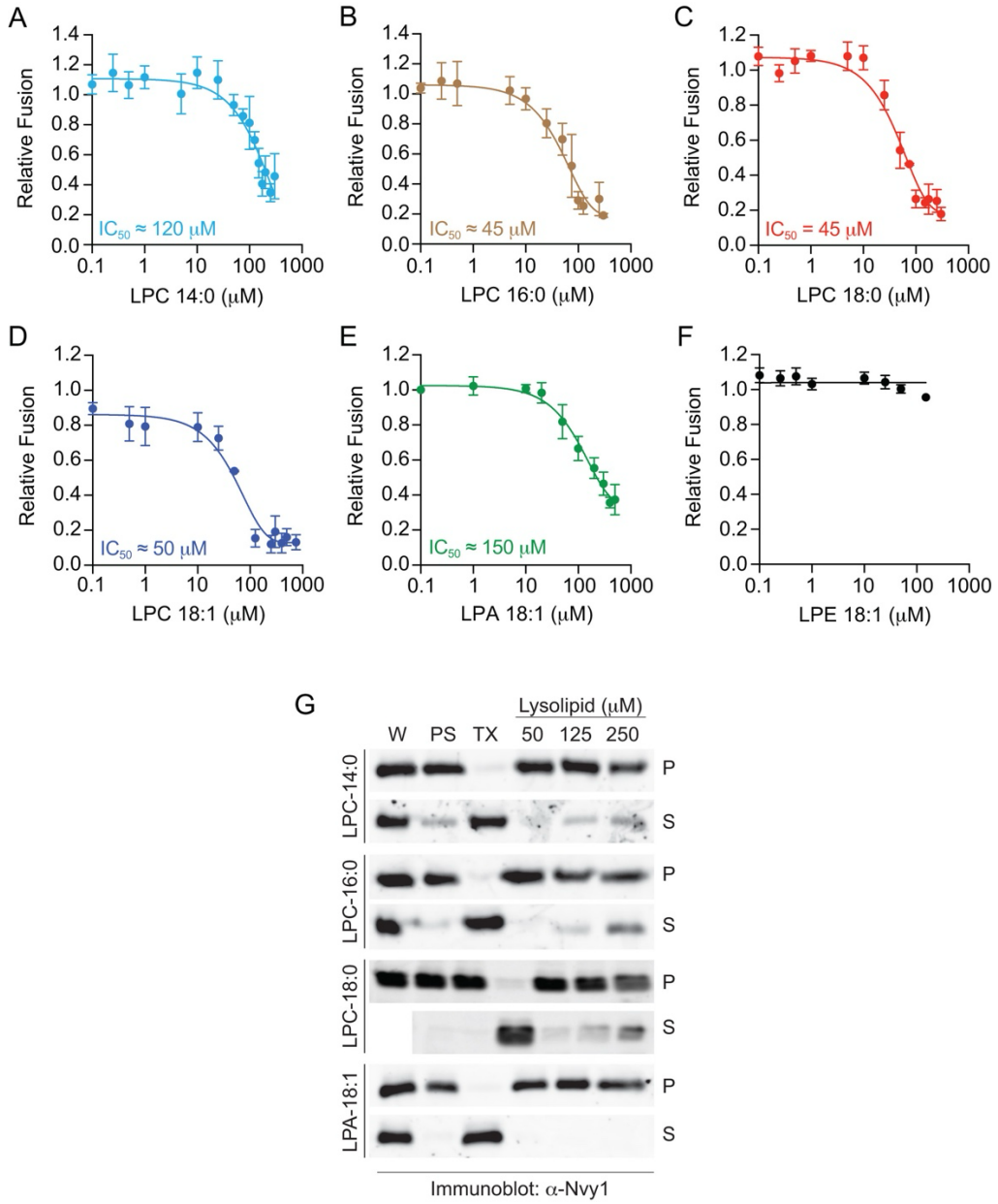

Figure 1. Inhibition of vacuole fusion by LPLs. Vacuole fusion reactions were treated with concentration curves of LPLs for 90 min at 27°C. Vacuole fusion reactions contained buffer or myristyl LPC 14:0 **(A)**, palmitoyl LPC 16:0 **(B),** stearoyl LPC 18:0 **(C)**, oleoyl LPC 18:1 **(D)**, oleoyl LPA 18:1 **(E),** or oleoyl LPE 18:1 **(F)**. Fusion values were normalized to the untreated control that is set to 1. Error bars represent mean ± SE. N≥3. **(G)** Purified vacuoles were incubated with PS buffer (PS), 1% Triton X-100 (TX), and LPL at the indicated concentrations. Reactions were incubated for 1 h at 30°C after which membranes were pelleted by centrifugation to separate vacuoles (P, pellet) from solubilized material (S, supernatant). Whole reactions (W), P and S were resolved by SDS-PAGE and immunoblotted for Nyv1.

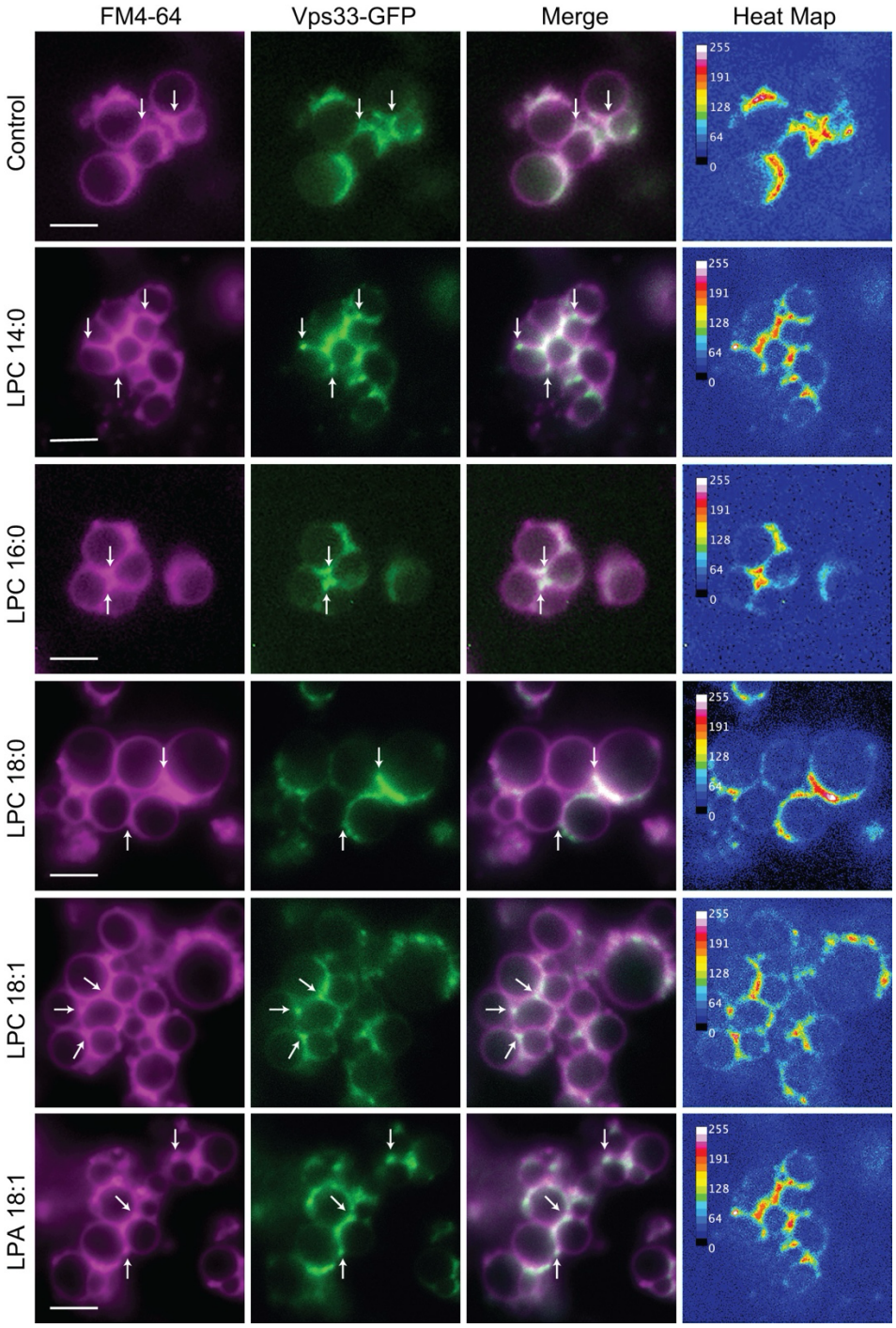

Figure 2. Purified vacuoles containing Vps33-GFP were treated with 50 μM LPC 16:0, LPC 18:0 and LPC 18:1, 150 μM LPC 14:0, 150 μM LPA 18:1 or buffer alone (control) and incubated for 30 min at 27°C. Limiting membranes were labeled with FM4-64. Vps33-GFP labeled vertex micro-domains. Shown are individual channels, merged images and heat maps to show GFP intensities. Arrows show vertex microdomain examples. Scale bar, 4 μm.

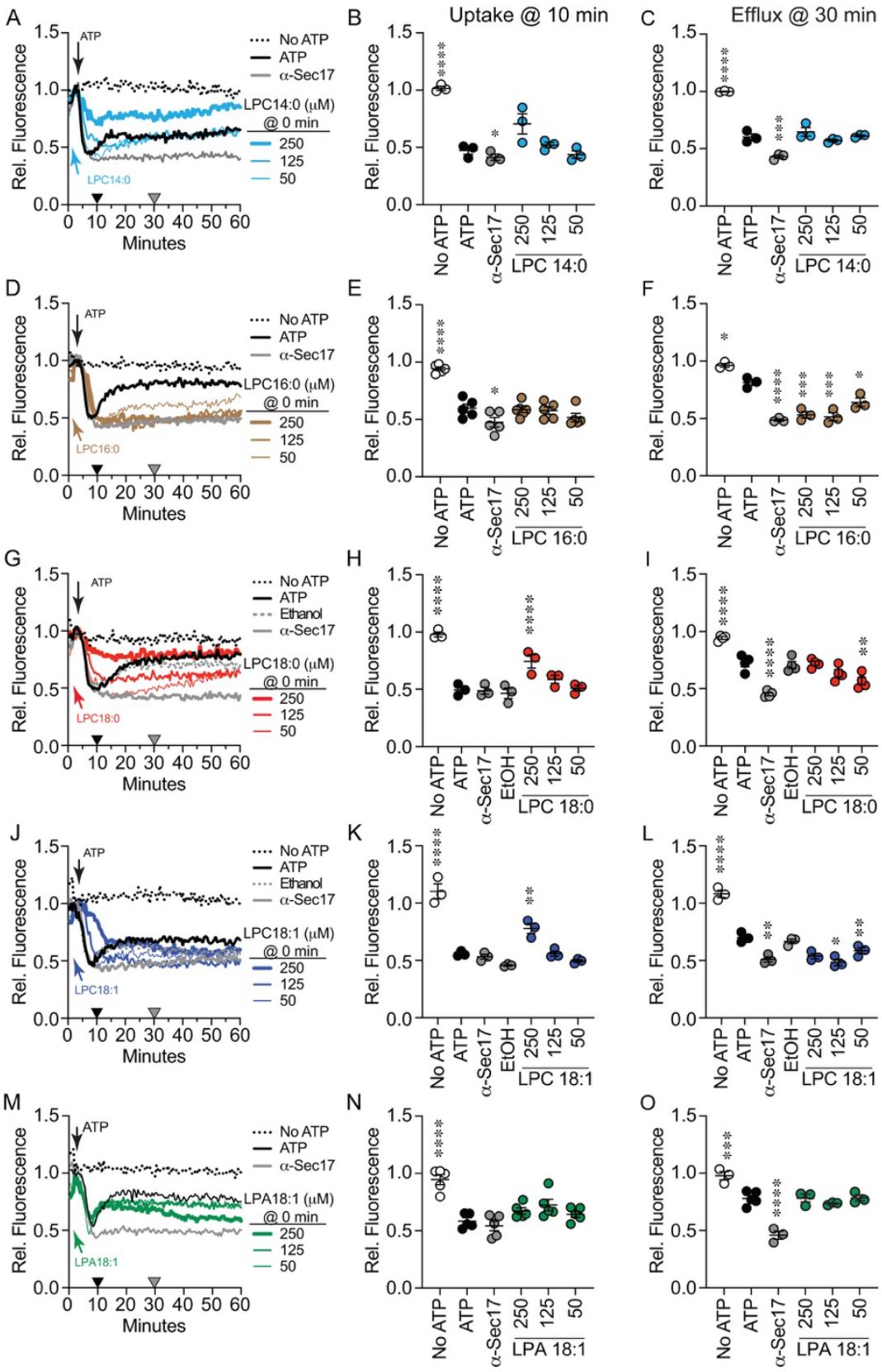
A
B
Uptake @ 10 min
C
Efflux @ 30 min
D
E
F
G
H
I
J
K
L
M
N
O
ATP
No ATP
ATP
Ethanol
α-Sec17
LPC14:0 (μM)
@ 0 min
LPC16:0 (μM)
LPC18:0 (μM)
LPC18:1 (μM)
LPA18:1 (μM)
250
125
50
LPC14:0
LPC16:0
LPC18:0
LPC18:1
LPA18:1
Rel. Fluorescence
Minutes
EtOH
LPC 14:0
LPC 16:0
LPC 18:0
LPC 18:1
LPA 18:1

914

915 **Figure 3. Effect of LPLs on Ca^{2+} uptake.** Vacuoles were isolated from BJ3505 and 2X fusion
916 reactions (60 µL) were treated with 140 µg/mL α-Sec17 IgG, LPC variants or reaction buffer at
917 T=0 min in the absence of ARS and in the presence of Cal-520. Reactions contained LPC 14:0
918 **(A)**, LPC 16:0 **(D)**, LPC 18:0 **(G)**, LPC 18:1 **(J)**, or LPA 18:1 **(M)**. After 5 min of incubation ARS or
919 buffer was added to each reaction. Cal-520 fluorescence was monitored every 30 s for 60 min.
920 Fluorescence values were normalized to the untreated control at T=5 when ATP was added and
921 set at 1. **(B, E, H, K, N)** Ca^{2+} uptake efficiency was quantified after 10 min of incubation (Black
922 triangles). **(C, F, I, L, O)** SNARE-dependent Ca^{2+} efflux efficiency was quantified after 30 min
923 incubation (Gray triangles). Data points represent mean ± SE ($n \geq 3$). Significance was measured
924 using one way ANOVA for multiple comparisons. Tukey's post hoc test was used for individual p
925 values. ***p<0.01, ****p<0.001, *****p<0.0001.
926

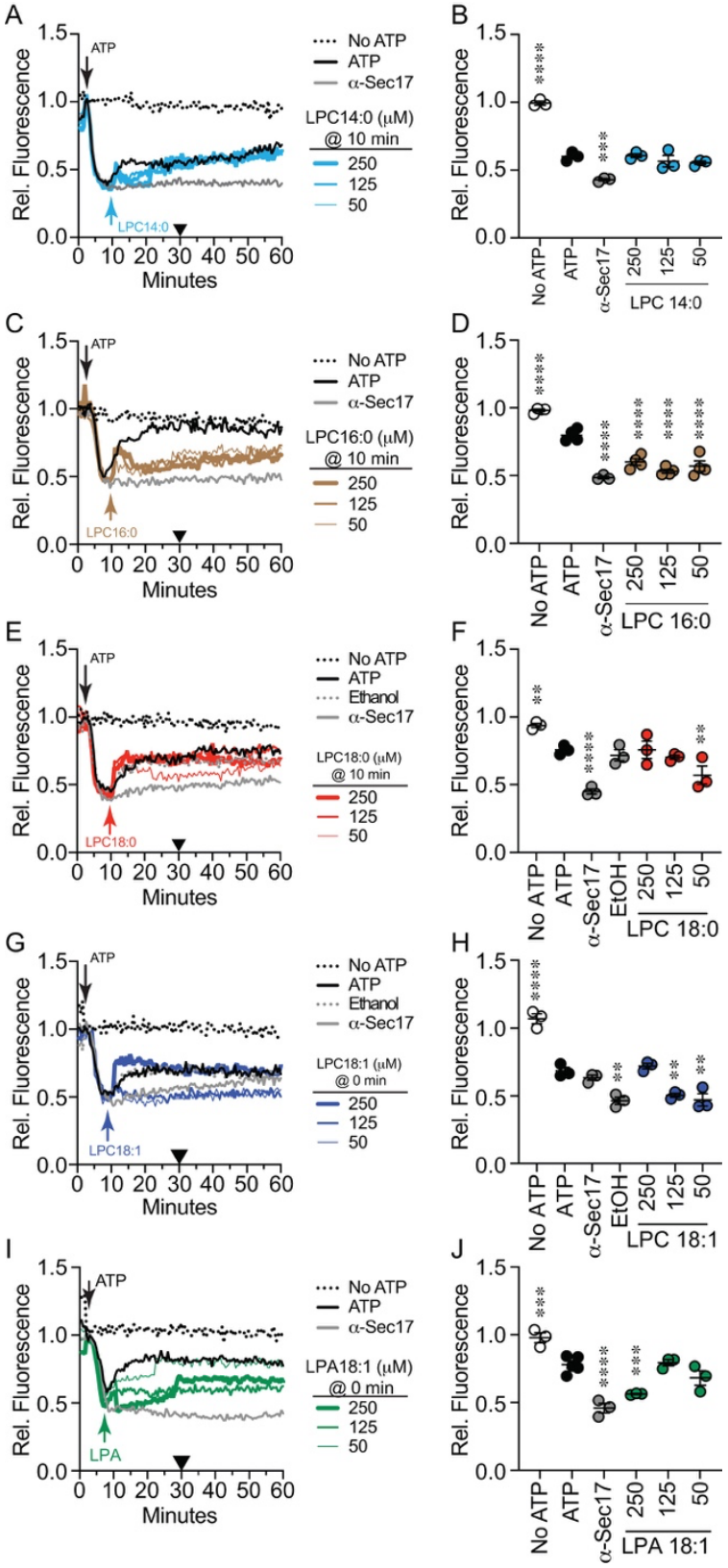
A
B
C
D
E
F
G
H
I
J
ATP
Rel. Fluorescence
Minutes
No ATP
ATP
α-Sec17
Ethanol
LPC14:0 (μM)
@ 10 min
LPC16:0 (μM)
@ 10 min
LPC18:0 (μM)
@ 10 min
LPC18:1 (μM)
@ 0 min
LPA18:1 (μM)
@ 0 min
250
125
50
LPC14:0
LPC16:0
LPC18:0
LPC18:1
LPA
EtOH
LPC 14:0
LPC 16:0
LPC 18:0
LPC 18:1
LPA 18:1

927

928

929 **Figure 4. Effect of LPLs on Ca^{2+} efflux.** Vacuoles from BJ3505 were incubated as 2X fusion
930 reactions (60 µL) and treated with 140 µg/mL α-Sec17 IgG at T=0 in the presence of Cal-520.
931 After 5 min of incubation ATP or buffer was added to each reaction. LPC variants were added
932 after 10 min. Reactions contained LPC 14:0 **(A)**, LPC 16:0 **(C)**, LPC 18:0 **(E)**, LPC 18:1 **(G)**, or
933 LPA 18:1 **(I)**. Cal-520 fluorescence was monitored every 30 s for 60 min. Fluorescence values
934 were normalized to the untreated control at T=5 min when ARS was added and set to 1. **(B, D, F,**
935 **H, J)** SNARE-dependent Ca^{2+} efflux efficiency was quantified after 30 min incubation (Black tri-
936 angles). Data points represent mean ± SE ($n \geq 3$). Significance was measured using one way
937 ANOVA for multiple comparisons. Tukey's post hoc test was used for individual p values. *$p<0.05$,
938 **$p<0.01$, ***$p<0.001$, ****$p<0.0001$.
939

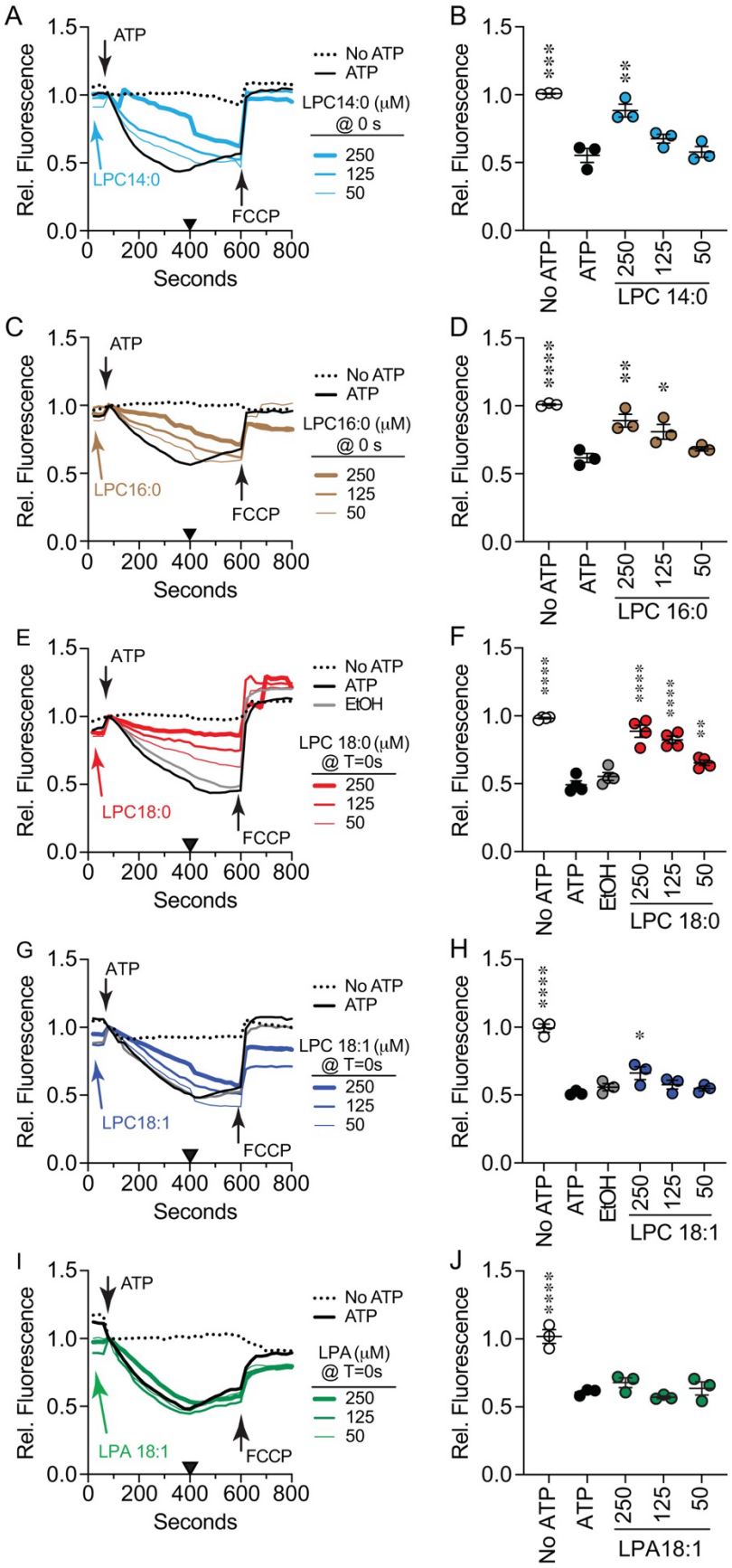
A
B
C
D
E
F
G
H
I
J
ATP
FCCP
No ATP
ATP
EtOH
LPC14:0 (μM) @ 0 s
LPC16:0 (μM) @ 0 s
LPC 18:0 (μM) @ T=0s
LPC 18:1 (μM) @ T=0s
LPA (μM) @ T=0s
250
125
50
LPC14:0
LPC16:0
LPC18:0
LPC18:1
LPA 18:1
Rel. Fluorescence
Seconds
LPC 14:0
LPC 16:0
LPC 18:0
LPC 18:1
LPA18:1

940

941 **Figure 5. Effect of LPLs on initial vacuole acidification.** BJ3505 vacuoles fusion reactions (2X)
942 were incubated with LPC variants or reaction buffer at T=0 min in the absence of ARS and in the
943 presence of AO. After 60 s of incubation received ARS or additional buffer and further incubated
944 for a total of 800 s. After 600 s each reaction received FCCP to equilibrate the proton gradient.
945 AO fluorescence was normalized to the fluoresced at the time of adding ARS and set to 1. Sepa-
946 rate experiments were treated with LPC 14:0 **(A)**, LPC 16:0 **(C)**, LPC 18:0 **(E)**, LPC 18:1 **(G)**, or
947 LPA-18:1 **(I). (B, D, F, H, J)** Vacuole acidification efficiency was quantified after 400 s (Black
948 triangles). Data ponts represent mean ± SE ($n \geq 3$). Significance was measured using one way
949 ANOVA for multiple comparisons. Tukey's post hoc test was used for individual p values. *$p<0.05$,
950 **$p<0.01$, ***$p<0.001$, ****$p<0.0001$.

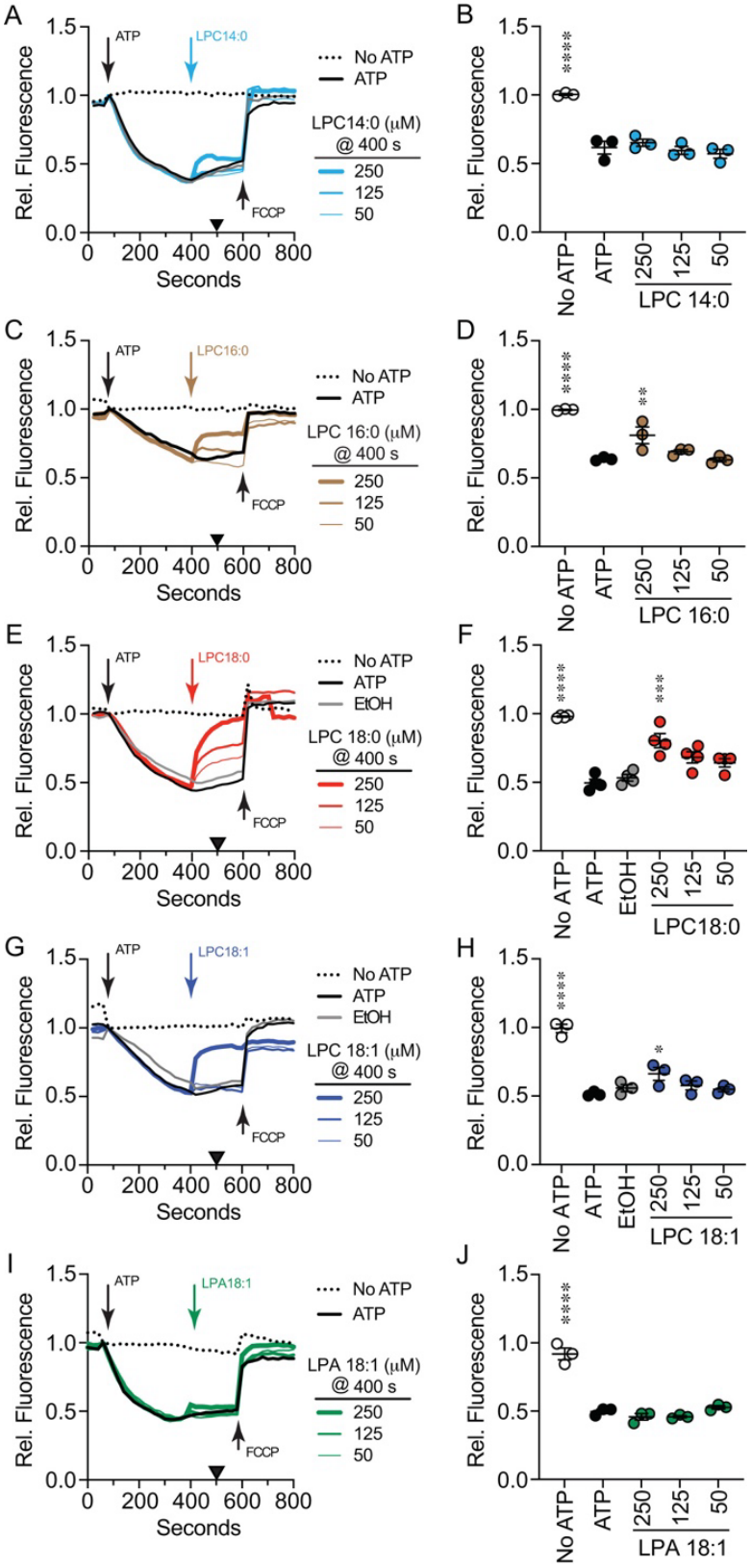
A
ATP
LPC14:0
No ATP
ATP
LPC14:0 (μM)
@ 400 s
250
125
50
FCCP
Rel. Fluorescence
Seconds
B
No ATP
ATP
250
125
50
LPC 14:0
C
LPC16:0
LPC 16:0 (μM)
D
LPC 16:0
E
LPC18:0
EtOH
LPC 18:0 (μM)
F
LPC18:0
G
LPC18:1
LPC 18:1 (μM)
H
LPC 18:1
I
LPA18:1
LPA 18:1 (μM)
J
LPA 18:1

951

952

953 **Figure 6. Effect of LPLs on maintaining vacuole acidification.** Vacuoles from BJ3505 were
954 incubated as 2X fusion reactions (60 µL) and incubated with reaction buffer and AO at T=0 min.
955 After 60 s of reactions received ARS or additional reaction buffer. LPC variants were added at
956 400 s. After 600 s each reaction received FCCP to equilibrate the proton gradient and further
957 incubated for a total of 800 s. AO fluorescence was normalized to the fluoresced at the time of
958 adding ARS and set to 1. Separate experiments were treated with LPC 14:0 **(A)**, LPC 16:0 **(C)**,
959 LPC 18:0 **(E)**, LPC 18:1 **(G)**, or LPA 18:1 **(I). (B, D, F, H, J)** Vacuole acidification efficiency was
960 quantified after 400 s (Black triangles). Data points represent mean ± SE ($n \geq 3$). Significance was
961 measured using one way ANOVA for multiple comparisons. Tukey's post hoc test was used for
962 individual p values. ***$p<0.001$, ****$p<0.0001$.
963
964

965 **Supplemental Information**

966

967 **Differential effects of lysophospholipid headgroups, acyl chain length and saturation on**

968 **vacuole acidification, Ca^{2+} transport, and fusion**

969

970

971 **Chi Zhang et al.**

972

973

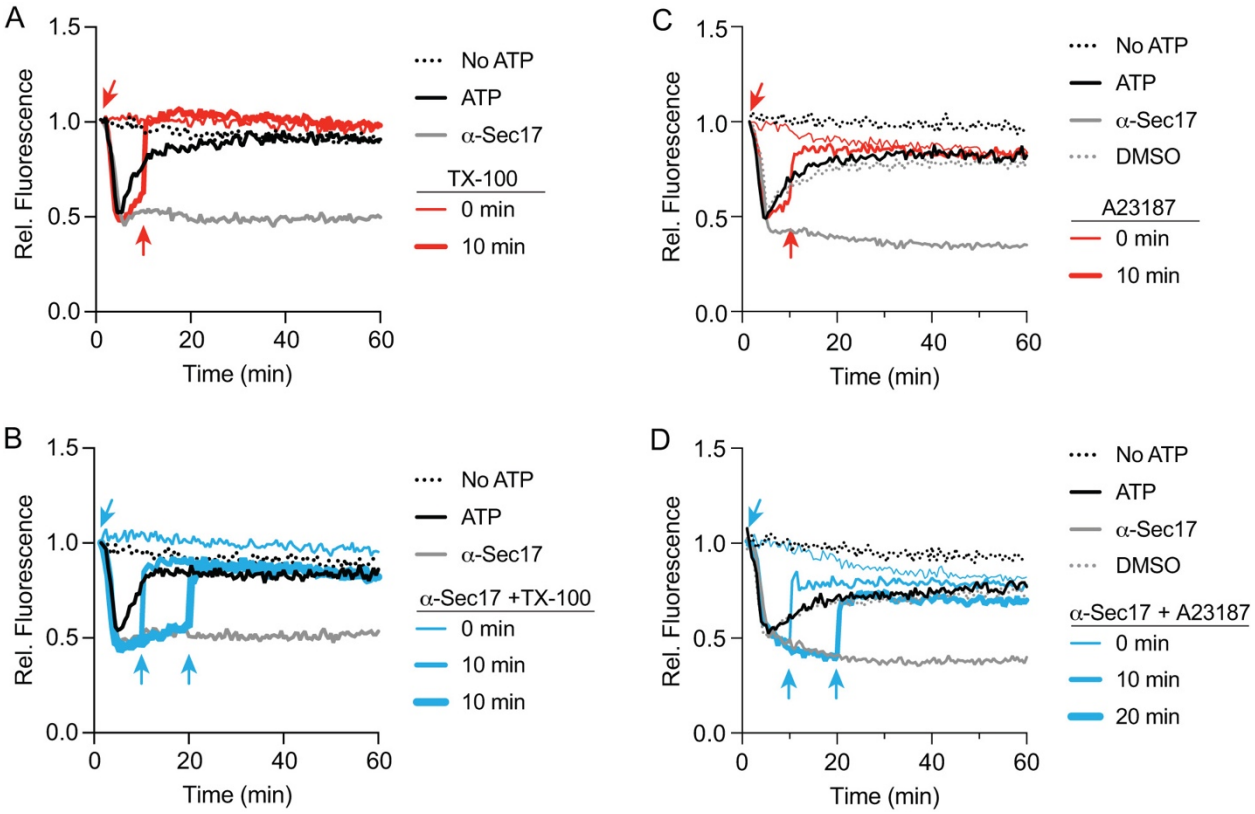

974
975
976
977 **Supplemental Figure 1. Effect of TX-100 and A23187 on Ca^{2+} transport.** Vacuoles were iso-
978 lated from BJ3505 were treated with 140 µg/mL α-Sec17 IgG, 1% TX-100, 100 µM A23187 or
979 PS added at T=0 or 10 min in the presence or absence of ARS and in the presence of Cal520.
980 **(A)** 1% TX-100 was added at T=0 or 10 min (red arrows). **(B)** 1% TX-100 was added to reac-
981 tions containing anti-Sec17 IgG at T=0 or 10 min (blue arrows). **(C)** 100 µM A23187 was added
982 at T=0 or 10 min (red arrows). **(B)** 100 µM A23187 was added to reactions containing anti-
983 Sec17 IgG at T=0 or 10 min.
984
985
986

987

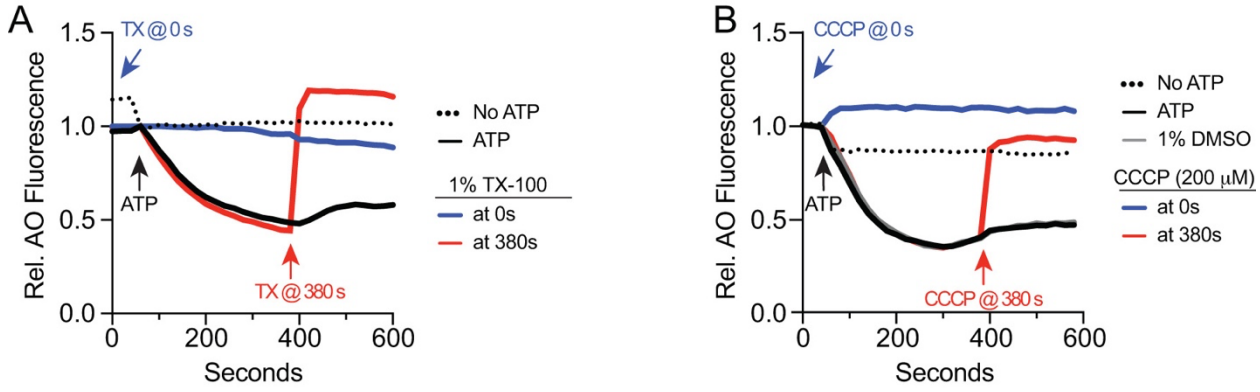

988
989
990
991 **Supplemental Figure 2. Effect of TX-100 or CCCP on vacuole acidification.** BJ3505 vacu-
992 oles fusion reactions (2X) were incubated with 1% TX-100 **(A)**, 200 μM CCCP **(B)** or reaction
993 buffer at T=0 or 380 sec in the presence or absence of ARS and in the presence of AO. After 60
994 s of incubation received ARS or additional buffer and further incubated for a total of 800 s. AO
995 fluorescence was normalized to the fluorescence at the time of adding ARS and set to 1.
996